Article

Immunity

NEMO Prevents RIP Kinase 1-Mediated Epithelial Cell Death and Chronic Intestinal Inflammation by NF-κB-Dependent and -Independent Functions

Graphical Abstract

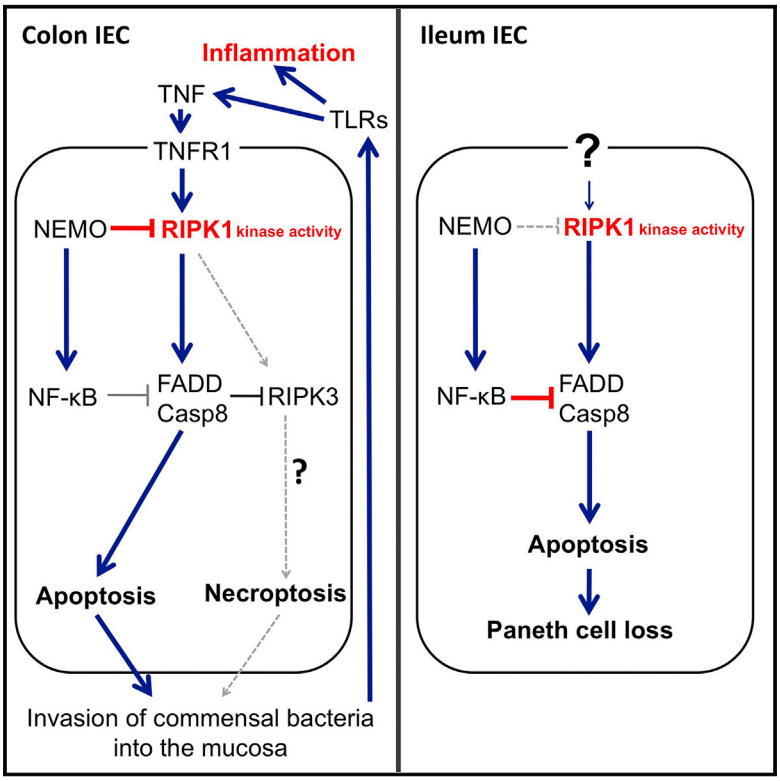

Highlights

- NEMO-mediated NF-κB signaling in the intestinal epithelium prevents Paneth cell death
- NF-κB-independent epithelial NEMO function prevents microbiota-driven colitis
- Combined FADD and RIPK3 deficiency prevents IEC death and colitis in NEMO^{IEC-KO} mice
- RIPK1-mediated death of IECs causes Paneth cell loss and colitis in NEMO^{IEC-KO} mice

Authors

Katerina Vlantis, Andy Wullaert, Apostolos Polykratis, ..., Ulf Klein, Michelle Kelliher, Manolis Pasparakis

Correspondence

pasparakis@uni-koeln.de

In Brief

The IKK-NF-κB-dependent mechanisms regulating intestinal epithelial homeostasis remain poorly understood. Pasparakis and colleagues show that NEMO prevents intestinal inflammation by inhibiting RIPK1-mediated intestinal epithelial cell death via NF-κB-dependent and -independent functions.

Vlantis et al., 2016, Immunity *44*, 553–567
March 15, 2016
http://dx.doi.org/10.1016/j.immuni.2016.02.020

Immunity
Article

NEMO Prevents RIP Kinase 1-Mediated Epithelial Cell Death and Chronic Intestinal Inflammation by NF-κB-Dependent and -Independent Functions

Katerina Vlantis,[1,2,3] Andy Wullaert,[1,2,3,8] Apostolos Polykratis,[1,2,3] Vangelis Kondylis,[1,2,3] Marius Dannappel,[1,2,3] Robin Schwarzer,[1,2,3] Patrick Welz,[1,2,3,9] Teresa Corona,[1,2,3] Henning Walczak,[4] Falk Weih,[5,10] Ulf Klein,[6] Michelle Kelliher,[7] and Manolis Pasparakis[1,2,3,*]

[1]Institute for Genetics, University of Cologne, 50674 Cologne, Germany
[2]Cologne Excellence Cluster on Cellular Stress Responses in Aging-Associated Diseases (CECAD), University of Cologne, 50931 Cologne, Germany
[3]Center for Molecular Medicine (CMMC), University of Cologne, 50931 Cologne, Germany
[4]Centre for Cell Death, Cancer and Inflammation (CCCI), UCL Cancer Institute, University College London, 72 Huntley Street, London WC1E 6D, UK
[5]Leibniz-Institute for Age Research, Fritz-Lipmann-Institute, 07745 Jena, Germany
[6]Herbert Irving Comprehensive Cancer Center, Departments of Pathology & Cell Biology and Microbiology & Immunology, Columbia University, New York, NY 10032, USA
[7]Department of Cancer Biology, University of Massachusetts Medical School, Worcester, MA 01605, USA
[8]Present address: Inflammation Research Center, VIB, and Department of Internal Medicine, Ghent University, Technologiepark 927, 9052 Ghent, Belgium
[9]Present address: Institute for Research in Biomedicine (IRB), 08028 Barcelona, Spain
[10]Deceased
*Correspondence: pasparakis@uni-koeln.de
http://dx.doi.org/10.1016/j.immuni.2016.02.020

SUMMARY

Intestinal epithelial cells (IECs) regulate gut immune homeostasis, and impaired epithelial responses are implicated in the pathogenesis of inflammatory bowel diseases (IBD). IEC-specific ablation of nuclear factor κB (NF-κB) essential modulator (NEMO) caused Paneth cell apoptosis and impaired antimicrobial factor expression in the ileum, as well as colonocyte apoptosis and microbiota-driven chronic inflammation in the colon. Combined RelA, c-Rel, and RelB deficiency in IECs caused Paneth cell apoptosis but not colitis, suggesting that NEMO prevents colon inflammation by NF-κB-independent functions. Inhibition of receptor-interacting protein kinase 1 (RIPK1) kinase activity or combined deficiency of Fas-associated via death domain protein (FADD) and RIPK3 prevented epithelial cell death, Paneth cell loss, and colitis development in mice with epithelial NEMO deficiency. Therefore, NEMO prevents intestinal inflammation by inhibiting RIPK1 kinase activity-mediated IEC death, suggesting that RIPK1 inhibitors could be effective in the treatment of colitis in patients with NEMO mutations and possibly in IBD.

INTRODUCTION

The maintenance of gut immune homeostasis depends on mechanisms regulating the interaction between the intestinal microbiota and host epithelial, stromal, and immune cells (Hooper et al., 2012; Kaser et al., 2010). The intestinal epithelium forms a physical and biochemical barrier between luminal bacteria and mucosal immune cells. It actively influences the intestinal microbiota by secreting anti-microbial factors and modulates mucosal immune responses via the production of immunoregulatory proteins (Hooper et al., 2012; Kaser et al., 2010). Paneth cells, specialized secretory intestinal epithelial cells found in small intestinal crypts, release peptides with anti-microbial activity that are believed to regulate the gut microbiota (Kaser et al., 2010; Ouellette, 2010). Deregulation of intestinal immune homeostasis results in chronic inflammatory bowel diseases, including Crohn's disease (CD) and ulcerative colitis (UC). Genetic, microbial, and environmental factors are thought to contribute to the pathogenesis of IBD; however, the mechanisms responsible for the initiation and chronicity of intestinal inflammation remain poorly understood (Blumberg and Powrie, 2012; Kaser et al., 2010).

Tumor necrosis factor (TNF) plays a critical role in intestinal inflammation as illustrated by the clinical efficacy of anti-TNF therapies in CD and UC (Peyrin-Biroulet, 2010). However, the TNF-dependent molecular and cellular mechanisms that contribute to the pathogenesis of IBD remain elusive. TNF signals primarily via TNF receptor 1 (TNFR1) to activate pro-survival and proinflammatory NF-κB and mitogen-activated protein kinase signaling or, when pro-survival responses are compromised, to induce cell death by FADD-Caspase-8-dependent apoptosis or RIPK3-mixed lineage kinase domain-like (MLKL)-mediated necroptosis (Pasparakis and Vandenabeele, 2015). RIPK1 is a key regulator of TNFR1 signaling that induces prosurvival and proinflammatory responses via kinase-independent scaffolding functions but also apoptosis or necroptosis via its

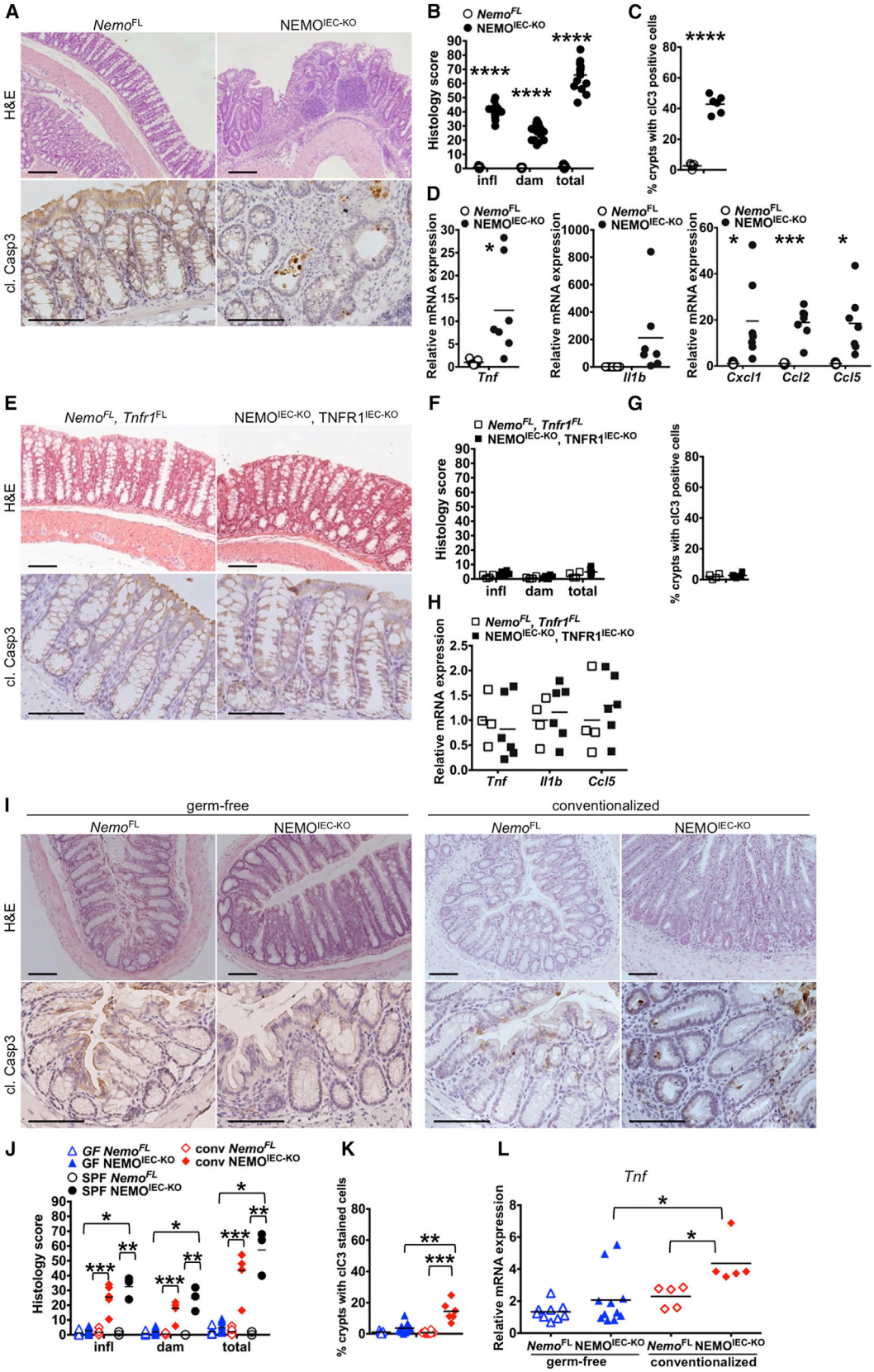

(legend on next page)

kinase activity (Pasparakis and Vandenabeele, 2015). Recent studies revealed the important role of kinase-independent RIPK1 functions in intestinal epithelial homeostasis (Dannappel et al., 2014; Dillon et al., 2014; Rickard et al., 2014; Takahashi et al., 2014), but the potential role of RIPK1 kinase activity in intestinal inflammation remains unknown.

The NF-κB pathway regulates immune and inflammatory responses. The NF-κB protein family consists of RelA, c-Rel, RelB, p50, and p52, which form hetero- and homodimers that control the transcription of NF-κB target genes by binding to consensus DNA sites in *cis*-regulatory regions (Oeckinghaus and Ghosh, 2009). RelA, c-Rel, and RelB have transcription transactivation domains, and hence NF-κB dimers containing these proteins are capable of activating gene expression (Oeckinghaus and Ghosh, 2009). p50 and p52 do not contain transactivation domains, and therefore p50 and p52 homodimers do not activate but rather suppress gene transcription. NF-κB dimers are kept inactive in resting cells by binding to inhibitor of NF-κB (IκB) proteins. The IκB kinase (IKK) complex, consisting of the NEMO (also named IKKγ) regulatory subunit and the IKK1 (also named IKKα) and IKK2 (also named IKKβ) kinases, activates NF-κB by phosphorylating IκB proteins, triggering their ubiquitin-dependent degradation and allowing the nuclear accumulation of NF-κB dimers and the transcription of target genes (Karin and Greten, 2005; Oeckinghaus and Ghosh, 2009).

Mice with IEC-specific NEMO deficiency develop spontaneous colitis that depends on MyD88 and TNFR1 signaling (Nenci et al., 2007). Interestingly, human patients with ectodermal dysplasia with immunodeficiency (EDA-ID) caused by hypomorphic NEMO mutations often suffer from colitis that is not resolved by hematopoietic stem cell transplantation (Fish et al., 2009; Kawai et al., 2012; Pai et al., 2008; Permaul et al., 2009), suggesting that NEMO deficiency in stromal cells also causes colon inflammation in humans. These results suggested that NEMO-mediated NF-κB activation in the intestinal epithelium is important for the maintenance of intestinal homeostasis in both mice and humans. However, mice lacking RelA in IECs do not develop spontaneous intestinal inflammation although they are highly sensitive to Dextran Sulfate Sodium (DSS)-induced colitis (Steinbrecher et al., 2008), questioning to which extent inhibition of NF-κB activation accounts for the disruption of intestinal epithelial homeostasis and the spontaneous development of colitis in mice with IEC-specific NEMO deficiency.

Here we show that NEMO exerts NF-κB-dependent and -independent functions that control intestinal homeostasis and inflammation by inhibiting RIPK1 kinase activity-dependent death of intestinal epithelial cells. These results revealed an important role of RIPK1 kinase activity in intestinal homeostasis, suggesting that RIPK1 kinase inhibitors could be effective for the treatment of gut inflammation in patients with NEMO mutations and might also prove beneficial in the therapy of IBD.

RESULTS

Epithelial TNFR1 Signaling and the Microbiota Drive Colitis in NEMO$^{IEC\text{-}KO}$ Mice

Mice lacking NEMO specifically in IECs (*Ikbkg*$^{fl/fl}$ or *Ikbkg*$^{fl/Y}$ *Villin-cre*$^{tg/WT}$, hereafter referred to as NEMO$^{IEC\text{-}KO}$) spontaneously developed chronic colitis, manifesting with diarrhea, thickening of the colonic wall, epithelial erosion, and ulcer formation, increased infiltration of immune cells in the mucosa and submucosa, and increased mRNA expression of pro-inflammatory cytokines and chemokines such as *Tnf*, *Il1b*, *Cxcl1*, *Ccl2*, and *Ccl5* (Figures 1A–1D). Increased numbers of apoptotic IECs, identified by staining for cleaved caspase-3, were detected in colonic crypts from NEMO$^{IEC\text{-}KO}$ mice (Figures 1A and 1C). We showed previously that systemic TNFR1 deficiency inhibited colitis development in NEMO$^{IEC\text{-}KO}$ mice (Nenci et al., 2007). To address whether IEC-intrinsic TNFR1 signaling triggered colitis in NEMO$^{IEC\text{-}KO}$ mice, we crossed them with mice carrying loxP-flanked TNFR1 alleles (*Tnfrsf1a*$^{fl/fl}$) (Van Hauwermeiren et al., 2013). IEC-specific knockout of TNFR1 prevented colonic epithelial cell death and the development of colitis in NEMO$^{IEC\text{-}KO}$ mice as shown by histological and cytokine expression analysis (Figures 1E–1H). Therefore, epithelial-intrinsic TNFR1 signaling induces colonocyte death and colitis in NEMO$^{IEC\text{-}KO}$ mice.

The death of NEMO-deficient IECs was proposed to trigger colitis in NEMO$^{IEC\text{-}KO}$ mice by disrupting the intestinal barrier allowing luminal bacteria to invade the mucosa and induce TLR-mediated inflammation (Nenci et al., 2007; Pasparakis, 2009). Indeed, NEMO$^{IEC\text{-}KO}$ mice raised under germ-free conditions did not develop colon inflammation and showed reduced numbers of apoptotic IECs (Figures 1I–1L, S1). Conventionalization of germ-free NEMO$^{IEC\text{-}KO}$ mice by co-housing with SPF mice resulted in the development of colitis within 2–4 weeks (Figures 1I–1L, S1). Thus, intestinal bacteria trigger colitis in NEMO$^{IEC\text{-}KO}$ mice.

Figure 1. Colitis in NEMO$^{IEC\text{-}KO}$ Mice Is Driven by the Microbiota and Epithelial TNFR1 Signaling

(A) Representative images of colon sections from NEMO$^{IEC\text{-}KO}$ and *Nemo*^{FL} littermates stained with H&E or immunostained for cleaved caspase-3 (cl. casp3).

(B) Graph depicting scores for inflammation (infl), tissue damage (dam), and overall histopathology of colon sections from NEMO$^{IEC\text{-}KO}$ and *Nemo*^{FL} mice (n = 11–16 mice per genotype).

(C) Graph depicting percentage of crypts with cl. casp. 3 stained cells on colon sections of NEMO$^{IEC\text{-}KO}$ and *Nemo*^{FL} mice (n = 5 or 6 mice per genotype).

(D) Graphs depicting mRNA levels of the indicated genes normalized to *Tbp* in the colon of NEMO$^{IEC\text{-}KO}$ and *Nemo*^{FL} mice (n = 7 mice per genotype).

(E) Representative images of colon sections from NEMO$^{IEC\text{-}KO}$ TNFR1$^{IEC\text{-}KO}$, and *Nemo*^{FL} *Tnfr1*^{FL} littermates.

(F) Graph depicting histopathological scores of colon sections from NEMO $^{IEC\text{-}KO}$ TNFR1$^{IEC\text{-}KO}$, and *Nemo*^{FL} *Tnfr1*^{FL} mice (n = 4–6 mice per genotype).

(G) Graph depicting percentage of crypts with cl. casp. 3 stained cells on colon sections of NEMO$^{IEC\text{-}KO}$ TNFR1$^{IEC\text{-}KO}$, and *Nemo*^{FL} *Tnfr1*^{FL} littermates (n = 4–6 mice per genotype).

(H) Graphs depicting mRNA levels of the indicated genes in the colon of NEMO$^{IEC\text{-}KO}$ TNFR1$^{IEC\text{-}KO}$, and *Nemo*^{FL} *Tnfr1*^{FL} mice (n = 4–6 mice per genotype).

(I) Representative images of colon sections from germ-free or germ-free NEMO$^{IEC\text{-}KO}$ and *Nemo*^{FL} mice 4 weeks after cohousing with SPF animals.

(J–L) Graphs depicting histopathological scores of colon sections, percentage of crypts with cl. casp. 3 stained colon IECs, and mRNA levels of *Tnf* in colons from germ-free, conventionalized, and SPF housed NEMO$^{IEC\text{-}KO}$ and *Nemo*^{FL} mice (n = 3–11 mice per genotype).

Scale bars represent 100 μm. See also Figure S1.

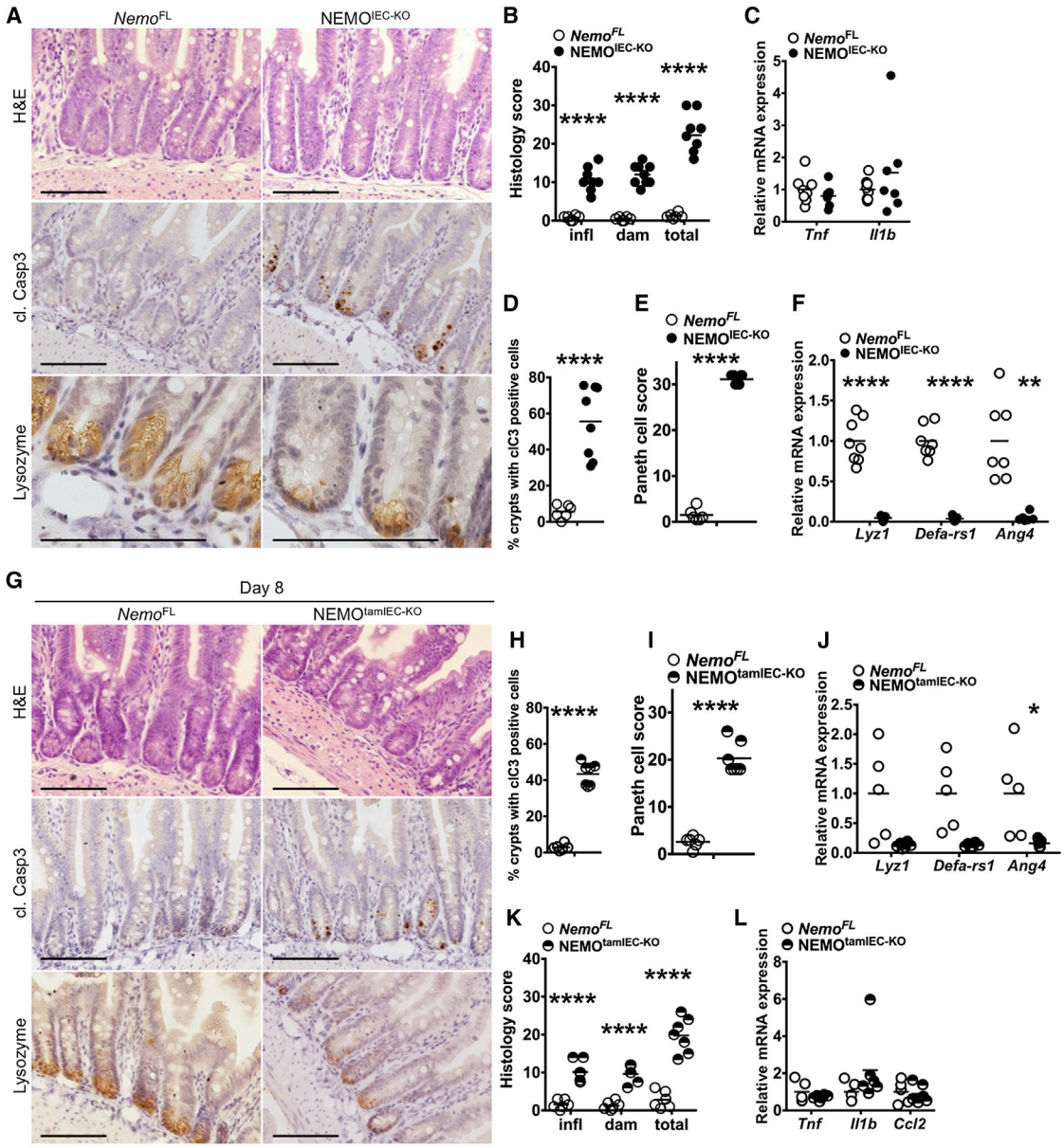

Figure 2. Reduced Paneth Cell Numbers and Increased IEC Apoptosis in Ileal Crypts of NEMO$^{IEC\text{-}KO}$ Mice

(A and G) Representative images of ileal sections from NEMO$^{IEC\text{-}KO}$ and *Nemo*^{FL}, NEMO$^{tamIEC\text{-}KO}$, and *Nemo*^{FL} littermates 8 days after tamoxifen administration stained with H&E or immunostained for cl. casp3 or lysozyme.

(B and K) Graph depicting histopathological scores of ileal sections from NEMO$^{IEC\text{-}KO}$ and *Nemo*^{FL}, NEMO$^{tamIEC\text{-}KO}$ and *Nemo*^{FL} littermates 8 days after tamoxifen administration (n = 6–9 mice per genotype).

(C, F, J, and L) Graphs depicting mRNA levels of the indicated genes in the ileum of NEMO$^{IEC\text{-}KO}$ and *Nemo*^{FL} mice and NEMO$^{tamIEC\text{-}KO}$ and *Nemo*^{FL} littermates 8 days after tamoxifen administration (n = 5–8 mice per genotype).

(D and H) Graphs depicting percentage of crypts with cl. casp. 3 stained IECs on ileal sections from NEMO$^{IEC\text{-}KO}$ and *Nemo*^{FL} mice and NEMO$^{tamIEC\text{-}KO}$ and *Nemo*^{FL} littermates 8 days after tamoxifen administration (n = 6–8 mice per genotype).

(E and I) Graphs depicting Paneth cell scores of ileal sections from NEMO$^{IEC\text{-}KO}$ and *Nemo*^{FL} mice and NEMO$^{tamIEC\text{-}KO}$ and *Nemo*^{FL} littermates 8 days after tamoxifen administration (n = 6–9 mice per genotype).

Scale bars represent 100 μm. See also Figure S2.

NEMO$^{IEC\text{-}KO}$ Mice Show a Severe Lack of Paneth Cells

The ileum of NEMO$^{IEC\text{-}KO}$ mice did not show epithelial erosion but had mildly increased immune cell infiltration although mRNA levels of *Tnf* and *Il1b* were not elevated (Figures 2A–2D, Figure S2A). Increased numbers of apoptotic IECs were almost exclusively detected in the crypt area and were rarely found in the villus. The number of Paneth cells, identified by their characteristic granule-filled morphology as well as by immunostaining

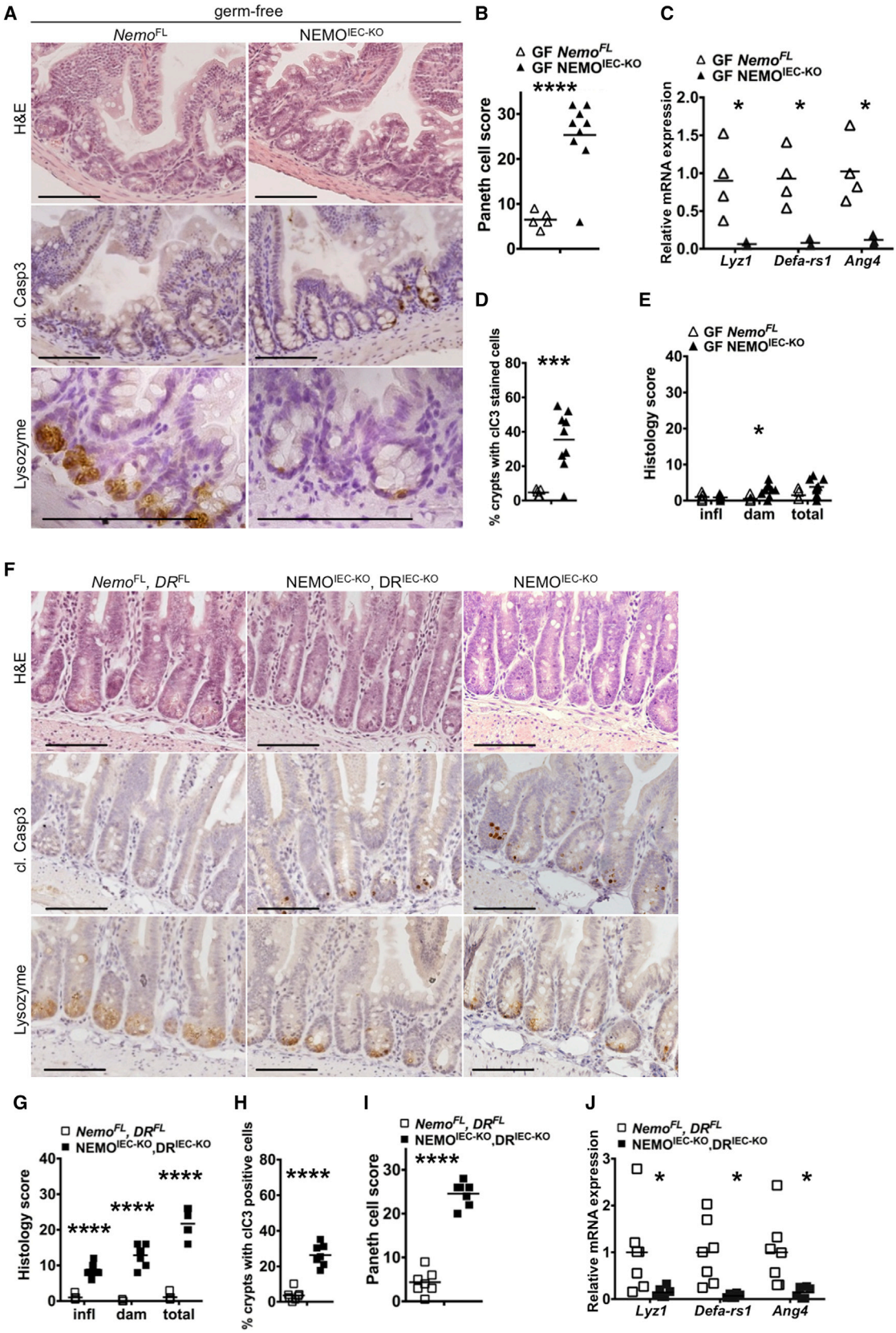

(legend on next page)

for lysozyme was strongly reduced in NEMO^{IEC-KO} mice (Figures 2A and 2E). In addition, NEMO^{IEC-KO} mice showed strongly reduced mRNA expression of anti-microbial factors produced specifically by Paneth cells including *Lyz1*, *Defa-rs1*, and *Ang4* (Figure 2F).

To assess whether the absence of Paneth cells in NEMO^{IEC-KO} mice reflected developmental or differentiation defects or whether it was caused by cell death, we employed mice allowing tamoxifen-inducible ablation of NEMO in IECs (*Ikbkg*$^{fl/fl}$ or *Ikbkg*$^{fl/Y}$ *Villin*-creERT2$^{tg/WT}$, hereafter referred to as NEMO$^{tamIEC-KO}$ mice). NEMO$^{tamIEC-KO}$ and *Nemo*^{fl} littermate controls that did not carry the *Villin*-creER^{T2} transgene were injected intraperitoneally with 1 mg tamoxifen on 5 consecutive days and were sacrificed on day 5 or day 8 for analysis. This protocol resulted in efficient NEMO ablation and activation of caspase-3 in IECs (Figure S2I). Immunostaining of ileal sections from NEMO$^{tamIEC-KO}$ mice sacrificed on day 5 did not reveal considerable tissue damage and inflammation or Paneth cell loss, although small numbers of apoptotic IECs were detected mainly in the crypt base (Figures S2B–S2D). However, 8 days after the first tamoxifen injection NEMO$^{tamIEC-KO}$ mice showed moderate tissue damage and immune cell infiltration, as well as strongly reduced numbers of Paneth cells and diminished expression of Paneth cell markers, accompanied by an increased number of apoptotic IECs in small intestinal crypts (Figures 2G–2K). Considering that Paneth cells are long lived with an estimated turnover time of about 60 days (Ireland et al., 2005), the finding that inducible NEMO deficiency resulted in Paneth cell loss within 8 days suggests that NEMO-deficient Paneth cells died, most likely by apoptosis as indicated by the presence of cleaved caspase-3-positive cells in intestinal crypts. Inflammatory cytokines and chemokines were not upregulated in the ileum of NEMO$^{tamIEC-KO}$ mice (Figure 2L), showing that the increased number of apoptotic IECs and the loss of Paneth cells did not trigger inflammation. Tamoxifen-inducible NEMO knockout caused increased IEC apoptosis, pronounced tissue damage, immune cell infiltration and strongly increased inflammatory cytokine and chemokine expression in the colon (Figures S2E–S2H). These results showed that epithelial NEMO deficiency caused Paneth cell death in ileal crypts.

Microbiota- and Death Receptor-Independent Paneth Cell Loss in NEMO^{IEC-KO} Mice

Our results presented above showed that epithelial intrinsic TNFR1 signaling induces the death of NEMO-deficient colonocytes triggering microbiota-driven colitis in NEMO^{IEC-KO} mice. To assess whether similar mechanisms contribute to Paneth cell loss in NEMO^{IEC-KO} mice, we first analyzed ileal tissue from germ-free animals. Paneth cell numbers and the expression of Paneth cell-derived antimicrobial factors was strongly reduced in germ-free NEMO^{IEC-KO} mice compared to *Nemo*^{FL} littermates (Figures 3A–3C). Moreover, germ free NEMO^{IEC-KO} mice showed IEC apoptosis in ileal crypts and tissue damage, albeit to a reduced extent compared to SPF mice (compare Figures 3D and 3E and 2A–2F).

We next asked whether TNFR1 signaling also triggered IEC death and Paneth cell loss in the small intestine of NEMO^{IEC-KO} mice. Examination of ileal sections from NEMO^{IEC-KO} TNFR1^{IEC-KO} mice revealed that IEC-specific TNFR1 deficiency did not diminish IEC apoptosis, tissue damage, and loss of Paneth cells (Figures S3A–S3E). To address whether Fas or TRAILR2, presumably acting in a redundant fashion with TNFR1, could be involved in triggering the death of NEMO-deficient Paneth cells, we generated NEMO^{IEC-KO} mice with simultaneous IEC-specific ablation of TNFR1, Fas, and TRAILR2 (*Ikbkg*$^{fl/fl}$ or *Ikbkg*$^{fl/Y}$ *Tnfrsf1a*$^{fl/fl}$ *Fas*$^{fl/fl}$ *Tnfrsf10b*$^{fl/fl}$ *Villin*-cre$^{tg/WT}$, hereafter referred to as NEMO^{IEC-KO} DR^{IEC-KO}) (Figures S3F–S3H). Even the combined loss of TNFR1, Fas and TRAILR2 could not prevent Paneth cell loss and tissue damage in ilea of NEMO^{IEC-KO} DR^{IEC-KO} animals, although it mildly reduced the number of apoptotic IECs (Figures 3F–3J, compare with Figures 2A–2F). Thus, Paneth cell loss in NEMO^{IEC-KO} mice occurred independently of the microbiota and death receptor signaling.

Combined Deficiency of FADD and RIPK3 Prevents Paneth Cell Loss and Colitis in NEMO^{IEC-KO} Mice

Most dying IECs in the intestine of NEMO^{IEC-KO} mice stained positive for cleaved caspase-3 suggesting that they die primarily by apoptosis. We therefore sought to address whether IEC apoptosis triggers the intestinal pathology of NEMO^{IEC-KO} mice by crossing them with mice carrying loxP-flanked alleles of FADD (*Fadd*$^{fl/fl}$), an adaptor protein that is essential for caspase-8-dependent apoptosis. NEMO^{IEC-KO} FADD^{IEC-KO} mice developed colitis and failed to thrive (data not shown), showing that FADD ablation did not prevent colon inflammation. As mice lacking FADD in IECs develop spontaneous colitis due to RIPK3-dependent epithelial cell necroptosis (Welz et al., 2011), we reasoned that necroptosis of IECs lacking both NEMO and FADD could trigger colitis in NEMO^{IEC-KO} FADD^{IEC-KO} mice. Indeed, NEMO^{IEC-KO} FADD^{IEC-KO} *Ripk3*$^{-/-}$ mice developed normally and did not show macroscopic signs of colitis. Histological analysis revealed a normal colonic mucosa without signs of epithelial erosion, tissue damage, and inflammatory cell infiltration (Figures 4A–4C), while proinflammatory genes were not

Figure 3. Paneth Cell Death in NEMO^{IEC-KO} Mice Is Independent of the Microbiota and Epithelial Death Receptor Signaling

(A and F) Representative images of ileal sections from germ-free NEMO^{IEC-KO} and *Nemo*^{FL} mice, and of SPF NEMO^{IEC-KO} DR^{IEC-KO} and *Nemo*^{FL} DR^{FL} mice.

(B and I) Graphs depicting Paneth cell scores of ileal sections from germ-free NEMO^{IEC-KO} and *Nemo*^{FL} mice, and of SPF NEMO^{IEC-KO} DR^{IEC-KO} and *Nemo*^{FL} DR^{FL} mice (n = 5–9 mice per genotype).

(C and J) Graphs depicting mRNA levels of the indicated genes in the ileum of germ-free NEMO^{IEC-KO} and *Nemo*^{FL} mice, and of SPF NEMO^{IEC-KO} DR^{IEC-KO} and *Nemo*^{FL} DR^{FL} mice (n = 3–7 mice per genotype).

(D and H) Graphs depicting the percentage of crypts with cl. casp. 3 stained cells on ileal sections from germ-free NEMO^{IEC-KO} and *Nemo*^{FL} mice, and of SPF NEMO^{IEC-KO} DR^{IEC-KO} and *Nemo*^{FL} DR^{FL} mice (n = 5–9 mice per genotype).

(E and G) Graphs depicting histopathological scores of ileal sections from germ-free NEMO^{IEC-KO} and *Nemo*^{FL} mice, and of SPF NEMO^{IEC-KO} DR^{IEC-KO} and *Nemo*^{FL} DR^{FL} mice (n = 5–9 mice per genotype).

Scale bars represent 100 μm. See also Figure S3.

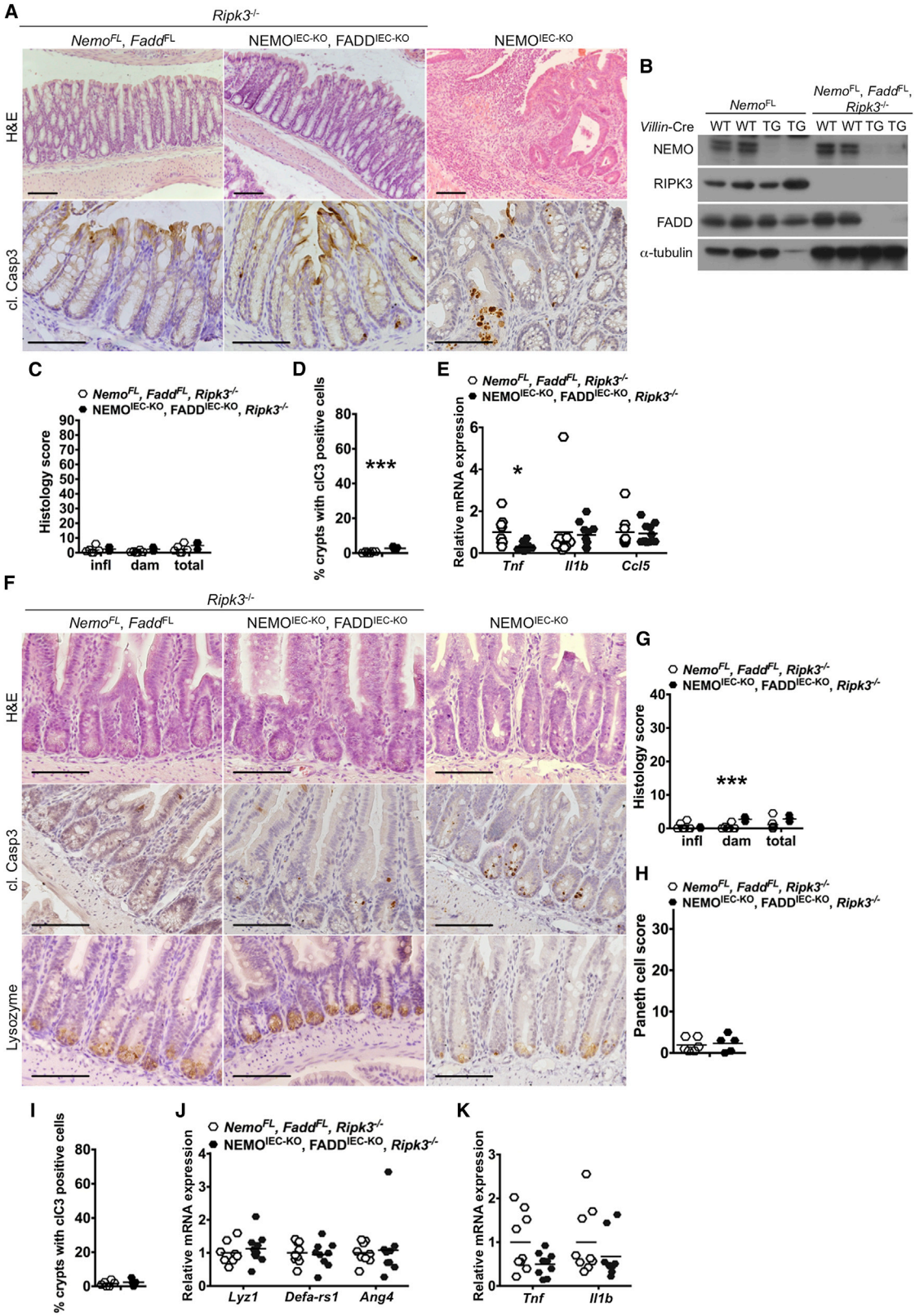

Figure 4. Combined Deficiency in FADD and RIPK3 Prevents IEC Death, Paneth Cell Loss, and Colitis in NEMO^{IEC-KO} Mice

(A and F) Representative images of colon and ileal sections from mice with the indicated genotypes.

(B) Immunoblot analysis of protein extracts from primary small intestinal IECs from mice with the indicated genotypes and with the indicated antibodies.

(legend continued on next page)

upregulated in the colons of NEMO^{IEC-KO} FADD^{IEC-KO} *Ripk3*$^{-/-}$ mice (Figure 4E). Moreover, NEMO^{IEC-KO} FADD^{IEC-KO} *Ripk3*$^{-/-}$ mice did not show Paneth cell loss in the ileum (Figures 4F–4K). A few scattered cells staining for cleaved caspase-3 were observed in the colon and ileum of NEMO^{IEC-KO} FADD^{IEC-KO} *Ripk3*$^{-/-}$ mice (Figures 4A, 4D, and 4F), but it is not clear whether these correspond to cells that escaped FADD deletion or cells undergoing FADD-independent apoptosis. These results showed that inhibition of apoptosis and necroptosis by combined ablation of FADD and RIPK3 fully protected NEMO^{IEC-KO} mice from Paneth cell loss and the development of colitis.

Because RIPK3 deficiency in the context of epithelial FADD knockout fully prevented intestinal pathology in NEMO^{IEC-KO} mice, we wondered whether RIPK3 might have a role independently of FADD. We therefore generated NEMO^{IEC-KO} *Ripk3*$^{-/-}$ mice and found that RIPK3 deficiency ameliorated the severity of colitis, with about 70% of the examined NEMO^{IEC-KO} *Ripk3*$^{-/-}$ animals (13 out of 17 mice analyzed at the age of 2–6 months) showing either overall mild inflammation affecting the entire colon or with only focal appearance of inflammatory lesions (Figures 5A and 5B). The remaining 30% of NEMO^{IEC-KO} *Ripk3*$^{-/-}$ mice developed severe pan-colitis that was histologically indistinguishable from the colitis observed in NEMO^{IEC-KO} mice (Figures 5A and 5B). Analysis of cytokine and chemokine expression confirmed that RIPK3 deficiency considerably inhibited inflammation in most NEMO^{IEC-KO} *Ripk3*$^{-/-}$ animals (Figure 5D, S4A). This variability was observed also within co-housed littermates suggesting that maternal or housing effects on the microbiota could not explain the incomplete penetrance of the protective effect provided by RIPK3 deficiency. The mechanisms responsible for the variability of colitis severity in NEMO^{IEC-KO} *Ripk3*$^{-/-}$ mice remain elusive at present and might be related to stochastic events precipitating disease in individual animals. Examination of ileal tissue from NEMO^{IEC-KO} *Ripk3*$^{-/-}$ mice revealed reduced Paneth cell numbers, decreased expression of Paneth cell markers and elevated numbers of apoptotic IECs, similarly to NEMO^{IEC-KO} mice (Figures 5E–5H and S4). Therefore, colitis development partly depends on RIPK3 while loss of Paneth cells occurs independently of RIPK3. It remains unclear whether RIPK3 modulates colitis by contributing to IEC death or by regulating inflammation in a cell-death independent manner.

RIPK1 Kinase Activity-Dependent Death of IECs Causes Colitis and Paneth Cell Loss in NEMO^{IEC-KO} Mice

To assess whether RIPK1 kinase activity contributes to IEC death and intestinal pathology in NEMO^{IEC-KO} mice, we crossed them with knockin mice expressing kinase inactive mutant RIPK1D138N (Polykratis et al., 2014). NEMO^{IEC-KO} *Ripk1*$^{D138N/D138N}$ mice showed a normal colonic mucosa without signs of inflammation, with only a few scattered apoptotic colonocytes detected (Figures 6A–6D). Moreover, lack of RIPK1 kinase activity also very strongly inhibited IEC apoptosis and loss of Paneth cells in the ileum of NEMO^{IEC-KO} *Ripk1*$^{D138N/D138N}$ mice (Figures 6E–6I).

To obtain insights on the mechanisms triggering the death of NEMO-deficient IECs, we assessed the formation of the FADD/Caspase-8 apoptosis-inducing signaling complex. Immunoprecipitation of FADD showed that Caspase-8 and RIPK1 strongly interacted with FADD in colon extracts from NEMO^{IEC-KO} but not *Nemo*^{FL} or NEMO^{IEC-KO} *Ripk1*$^{D138N/D138N}$ mice (Figure 6J). These findings indicate that NEMO deficiency triggers the RIPK1 kinase activity-dependent formation of a RIPK1/FADD/Caspase-8 signaling complex that induces apoptosis in IECs. Collectively, these findings show that RIPK1 kinase activity-mediated death of IECs causes Paneth cell loss and colitis development in NEMO^{IEC-KO} mice.

Epithelial NF-κB Deficiency Causes RIPK1 Kinase-Dependent Paneth Cell Loss but Does Not Trigger Colitis

To address whether epithelial NEMO deficiency causes intestinal pathology by inhibiting NF-κB activation, we sought to directly inhibit NF-κB by generating mice with IEC-specific knockout of NF-κB subunits. As reported earlier (Steinbrecher et al., 2008), mice with IEC-specific RelA deficiency (*Rela*$^{fl/fl}$ *Villin-cre*$^{tg/WT}$, hereafter referred to as RelA^{IEC-KO}) did not develop spontaneous colitis (Figures S5A–S5D). However, RelA^{IEC-KO} mice showed increased IEC apoptosis and reduced Paneth cell numbers in ileal crypts, as well as reduced expression of Paneth-cell-specific genes (Figures 7A–7E). RelA^{IEC-KO} *Ripk1*$^{D138N/D138N}$ mice did not exhibit IEC death and loss of Paneth cells (Figures 7A–7E), showing that RIPK1 kinase activity induces Paneth cell death also in RelA^{IEC-KO} mice.

The absence of spontaneous colitis in RelA^{IEC-KO} mice could be due to compensation of RelA function by other NF-κB subunits. To address potential redundancies among NF-κB factors, we generated mice lacking all three Rel proteins capable to activate gene transcription (namely RelA, RelB, and c-Rel) specifically in IECs (*Rela*$^{fl/fl}$ *Relb*$^{fl/fl}$ *c-Rel*$^{fl/fl}$ *Villin-cre*$^{tg/WT}$, hereafter referred to as NF-κB^{IEC-KO} mice) (Figure S5F). Combined lack of RelA, c-Rel, and RelB as well as NEMO deficiency blunted TNF-induced expression of NF-κB-dependent genes demonstrating efficient inhibition of NF-κB responses (Figure S5H). In contrast to NEMO^{IEC-KO}, NF-κB^{IEC-KO} animals did not develop spontaneous colitis although small numbers of cleaved caspase-3 positive epithelial cells and mild inflammation were detected in the colon of some of these mice (Figures 7F–7I). Thus, even complete inhibition of NF-κB activity in the intestinal epithelium was not sufficient to trigger spontaneous colitis development, suggesting that NEMO prevents colitis via NF-κB-independent functions. Similarly to RelA^{IEC-KO}, NF-κB^{IEC-KO} mice showed elevated numbers of apoptotic IECs and Paneth cell loss in ileal crypts (Figures 7J–7N). However, Paneth cell loss in NF-κB^{IEC-KO} or RelA^{IEC-KO} mice was not as severe as in NEMO^{IEC-KO} mice suggesting that inhibition of NF-κB

(C and G) Graphs depicting histopathological scores of colon and ileal sections from mice with the indicated genotypes (n = 5 or 6 mice per genotype).
(D and I) Graphs depicting the percentage of crypts with cl. casp. 3 stained cells on colon and ileal sections from littermates with the indicated genotypes (n = 5 or 6 mice per genotype).
(E, J, and K) Graphs depicting mRNA levels of the indicated genes in the colon and ileum of mice with the indicated genotypes (n = 9 or 10 mice per genotype).
(H) Graph depicting Paneth cell scores of ileal sections from mice with the indicated genotypes (n = 5 or 6 mice per genotype).
Scale bars represent 100 μm.

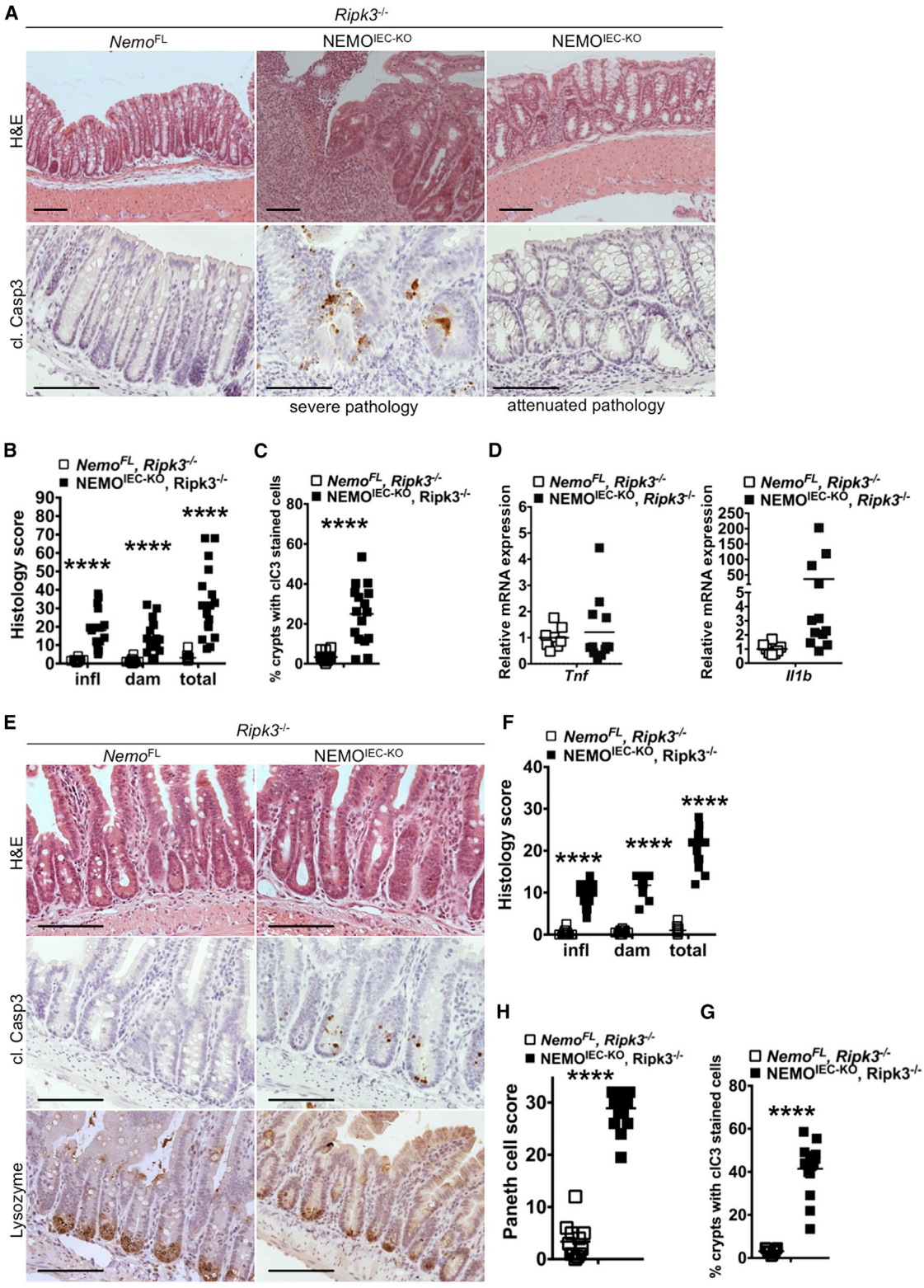

Figure 5. RIPK3 Deficiency Ameliorates Colitis but Does Not Prevent Paneth Cell Loss in NEMO^{IEC-KO} Mice

(A and E) Representative images of colon and ileal sections from mice with the indicated genotypes.

(B and F) Graphs depicting histopathological scores of colon and ileal sections from mice with the indicated genotypes (n = 12–17 mice per genotype).

(legend continued on next page)

activation can only partly explain the loss of Paneth cells in NEMO^{IEC-KO} mice. These results suggest that NF-κB activity inhibits Paneth cell apoptosis in the ileum, but NF-κB-independent NEMO functions prevent IEC death and chronic inflammation in the colon.

RIPK1 Kinase Activity Mediates Embryonic Lethality in RelA and NEMO Knockout Mice

To address whether the TNF-dependent embryonic lethality of *Rela*$^{-/-}$ mice also depends on RIPK1 kinase activity, we crossed them to *Ripk1*$^{D138N/D138N}$ animals. *Rela*$^{-/-}$ *Ripk1*$^{D138N/D138N}$ mice were born, albeit at somewhat reduced numbers compared to the expected Mendelian ratio, but died during the first weeks of life (Figure S6) most likely due to infections as previously shown for *Rela*$^{-/-}$ *Tnfr1*$^{-/-}$ mice (Alcamo et al., 2001). Moreover, we found that NEMO-deficient mice were also born, though at reduced ratio, in the *Ripk1*$^{D138N/D138N}$ genetic background (Figure S6). Therefore, the embryonic lethality evoked by NEMO or RelA deficiency is caused, at least in part, by RIPK1 kinase activity-dependent TNF-induced death of cells in the fetal liver, suggesting that NF-κB activity is essential during embryogenesis to restrain RIPK1-dependent cell death.

DISCUSSION

Deregulation of intestinal epithelial responses to the microbiota and the cytokine microenvironment of the gut are believed to contribute to the pathogenesis of inflammatory bowel diseases (Blumberg and Powrie, 2012; Hooper et al., 2012; Kaser et al., 2010). The NF-κB pathway controls cellular responses to microbes and cytokines and a number of studies suggested that NF-κB activation in IECs controls intestinal immune homeostasis (Eckmann et al., 2008; Nenci et al., 2007; Steinbrecher et al., 2008; Zaph et al., 2007). Particularly the finding that NEMO^{IEC-KO} mice develop spontaneous colitis suggested that epithelial NF-κB signaling is essential to prevent colon inflammation (Nenci et al., 2007). NF-κB subunit redundancy and the embryonic lethality of RelA-deficient mice made it difficult to address the functional role of NF-κB signaling in the gut. To overcome these limitations, we employed conditional targeting of all NF-κB subunits capable of transcriptional activation, namely RelA, c-Rel, and RelB, to generate mice lacking NF-κB activity in the intestinal epithelium. Our studies revealed that even complete inhibition of NF-κB in IECs did not cause spontaneous colitis as seen in the NEMO^{IEC-KO} mice, demonstrating that NF-κB activity in IECs is not essential to prevent colon inflammation under steady-state conditions. In contrast, NF-κB inhibition caused IEC death and Paneth cell loss in the small intestine similarly to NEMO knockout. These results revealed a divergence of IKK-NF-κB signaling in the gut. NEMO-mediated NF-κB activation inhibits the death of IECs and loss of Paneth cells in the small intestine, while NF-κB-independent NEMO functions prevent IEC death and inflammation in the colon.

The potentially differential role of apoptosis and necroptosis in regulating inflammation has been the subject of debate. Apoptosis is believed to be less inflammatory than necroptosis due to the limited release of DAMPs by apoptotic cells (Pasparakis and Vandenabeele, 2015), although the consequences of these distinct types of regulated cell death in the intestinal epithelium remain poorly understood. Most dying IECs in the NEMO^{IEC-KO} mice stained for cleaved caspase-3, suggesting that they died by apoptosis. Due to the absence of a reliable marker for the identification of necroptotic cells in mouse tissues, we were not able to assess and quantify the occurrence of necroptosis in these mice. Our efforts to genetically dissect the contribution of apoptosis and necroptosis of IECs in NEMO^{IEC-KO} mice also did not lead to unambiguous results. We attempted to specifically address the contribution of IEC apoptosis by generating mice lacking both NEMO and FADD in the intestinal epithelium and found that these mice developed intestinal inflammation. IEC death, Paneth cell loss, and colitis development in NEMO^{IEC-KO} mice were fully prevented by FADD epithelial knockout combined with systemic RIPK3 deficiency, showing that inhibition of both apoptotic and necroptotic death of IECs protects these mice from intestinal pathology. However, since FADD epithelial deficiency caused IEC necroptosis and colitis in mice (Welz et al., 2011), a likely interpretation of these findings is that FADD knockout might prevent apoptosis of NEMO-deficient IECs, but at the same time renders them susceptible to RIPK3-dependent necroptosis. RIPK3 deficiency alone did not prevent Paneth cell loss but partially ameliorated colitis severity in NEMO^{IEC-KO} mice. These results show that necroptosis is not involved in IEC death in the small intestine but indicate that it could be partly implicated in the death of colonocytes and colitis development in these mice. However, RIPK3 has been suggested to also mediate apoptosis as well as cell-death-independent functions relevant for inflammation. A recent study reported that RIPK3 deficiency exacerbated DSS-induced colitis, which was attributed to a function of RIPK3 in promoting the expression of cytokines required for efficient injury repair in dendritic cells (Moriwaki et al., 2014). This proposed anti-inflammatory function of RIPK3 opposes its predominantly pathogenic role in the NEMO^{IEC-KO} mice and is therefore unlikely to contribute to the amelioration of colitis in NEMO^{IEC-KO} *Ripk3*$^{-/-}$ mice. Furthermore, RIPK3 has been suggested to regulate inflammasome activation and IL-1β release in a necroptosis-independent manner (Kang et al., 2013; Lawlor et al., 2015; Wang et al., 2014). Therefore, because of the complex and as-yet incompletely understood functions of RIPK3 in cell death and inflammation, at this stage it is unclear whether RIPK3 deficiency ameliorates colitis in NEMO^{IEC-KO} mice by inhibiting necroptosis or apoptosis or other proinflammatory RIPK3 functions. Further experiments will be required to dissect the potential role of necroptosis in the development of colitis in NEMO^{IEC-KO} mice.

Our results provide in vivo experimental evidence that RIPK1 kinase activity-dependent death of NEMO-deficient epithelial

(C and G) Graphs depicting the percentage of crypts with cl. casp. 3 stained cells on colon and ileal sections from littermates with the indicated genotypes (n = 11–16 mice per genotype).
(D) Graphs depicting mRNA levels of the indicated genes in the colon of mice with the indicated genotypes (n = 8–12 mice per genotype).
(H) Graph depicting Paneth cell scores of ileal sections from mice with the indicated genotypes (n = 12–17 mice per genotype).
Scale bars represent 100 μm. See also Figure S4.

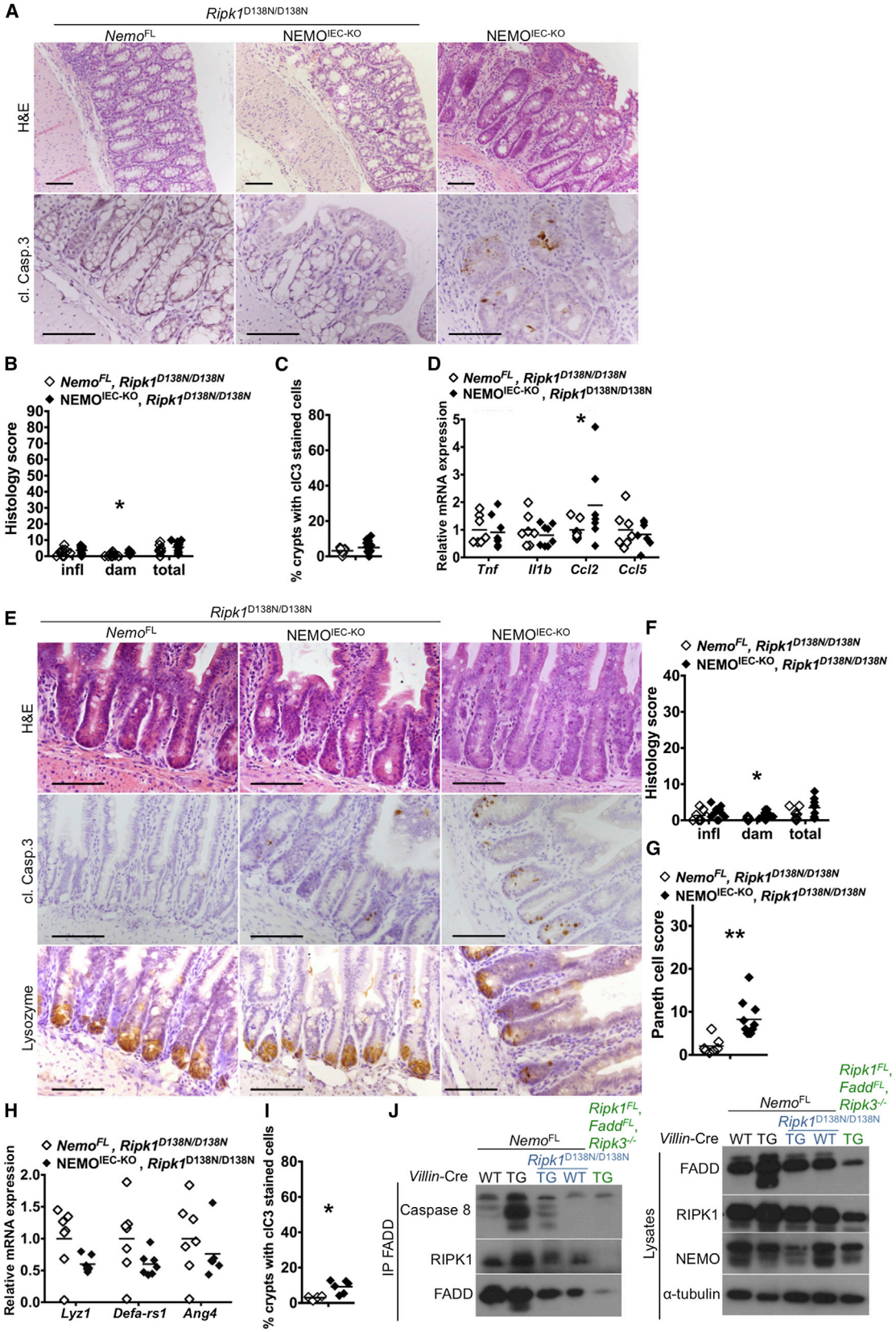

(legend on next page)

cells triggers Paneth cell loss in the small intestine and severe chronic inflammation in the colon. Different mechanisms trigger RIPK1-dependent epithelial cell death in the small and large intestine. TNFR1-mediated death of IECs causes microbiota-dependent inflammation in the colon. In contrast, IEC death and loss of Paneth cells occurs in the combined absence of TNFR1, Fas and TRAILR2, and does not require the presence of the microbiota, although germ-free conditions ameliorated the pathology indicating that intestinal bacteria contribute to the severity of the ileal phenotype. The upstream stimuli inducing IEC death in ileal crypts in NEMO^{IEC-KO} mice remain unclear. TRIF-dependent TLR signaling, but also type I and type II interferon receptors have been shown to induce RIPK1-dependent cell death, suggesting that these receptors might contribute to the death of NEMO-deficient enterocytes.

The molecular mechanisms by which NEMO and NF-κB signaling prevent RIPK1-mediated IEC death remain unclear. Earlier in vitro studies in cell lines suggested that NEMO interacts with RIPK1 via its ubiquitin-binding domain and prevents the engagement of FADD/caspase-8 to trigger apoptosis (Legarda-Addison et al., 2009) or, when caspase 8 is inhibited, necroptosis (O'Donnell et al., 2012). However, in these in vitro studies RIPK1 kinase activity was suggested to be required for necroptosis but not for apoptosis of NEMO deficient cells (O'Donnell et al., 2012), while our results suggest that RIPK1 causes intestinal pathology primarily by inducing IEC apoptosis. A recent study suggested that IKK1 and IKK2 prevent TNF-induced cell death by directly phosphorylating RIPK1 and inhibiting RIPK1-induced death signaling independently of NF-κB, and proposed that loss of IKK1/2 or NEMO causes RIPK1-dependent death while NF-κB inhibition causes RIPK1-independent cell death downstream of TNFR1 signaling (Dondelinger et al., 2015). However, our results showing that RIPK1 kinase activity mediates death of NEMO- or p65-deficient IECs but also embryonic lethality of NEMO- or p65-deficient mice provide in vivo experimental evidence that NF-κB signaling also controls RIPK1-mediated cell death. These results suggest that IKK/NF-κB signaling acts at multiple levels both by directly interacting with upstream components of the cell death machinery such as RIPK1, but also by inducing the expression of pro-survival genes. NEMO could directly bind RIPK1 via its ubiquitin binding domain and this interaction might be important to prevent the formation of the RIPK1-containing signaling complex. Indeed, our immunoprecipitation experiments suggested that NEMO deficiency triggers the formation of a RIPK1/FADD/caspase-8 apoptosis-inducing signaling complex. Further studies will be required to dissect the IKK- and NF-κB-dependent mechanisms regulating RIPK1-induced cell death.

Loss of Paneth cells is frequently observed in CD and might be functionally implicated in the development of intestinal inflammation in these patients, presumably by inducing dysbiosis (Blumberg and Powrie, 2012; Kaser et al., 2010). Our results showing that RelA^{IEC-KO} mice exhibit extensive loss of Paneth cells but do not develop spontaneous intestinal inflammation suggest that death of Paneth cells is not sufficient to disrupt homeostasis and cause ileitis or colitis even in the presence of an underlying NF-κB defect in the intestinal epithelium. However, although Paneth cell loss is not sufficient by itself to cause the disease, it might contribute to the development of colitis in NEMO^{IEC-KO} mice.

Human patients with hypomorphic NEMO mutations develop ectodermal dysplasia accompanied with severe immunodeficiency (EDA-ID) and about 25% of these patients suffer from inflammatory colitis (Hanson et al., 2008; Kawai et al., 2012). Hematopoietic stem cell transplantation (HSCT) has been used for the treatment of immunodeficiency in EDA-ID patients (Fish et al., 2009; Pai et al., 2008). Although HSCT could successfully restore immune function, it did not improve but rather worsened colitis (Fish et al., 2009; Pai et al., 2008), suggesting that stromal NEMO deficiency causes colitis in human EDA-ID patients similarly to our mouse model with epithelial specific NEMO knockout. TNF neutralizing antibodies were effective in treating colitis in EDA-ID (Mizukami et al., 2012), showing that similarly to NEMO^{IEC-KO} mice, TNF causes colitis in the human patients. However, considering the impaired immune function of NEMO EDA-ID patients, additional treatment with anti-TNF increases the risk of serious bacterial infections. Our results that inhibition of RIPK1 kinase activity prevented the development of intestinal pathology in NEMO^{IEC-KO} mice suggest that RIPK1 kinase inhibitors could be highly effective for the treatment of gastrointestinal complications in human patients with EDA-ID caused by NEMO mutations, in particular after successful restoration of immune function by HSCT. Because knockin mice expressing kinase inactive RIPK1 do not show any abnormalities, RIPK1 kinase inhibitors are expected to be well tolerated and should therefore be superior to anti-TNF treatment for these patients. Intestinal epithelial cell death is commonly observed in patients with inflammatory bowel diseases, including CD and UC (Seidelin and Nielsen, 2009; Souza et al., 2005). Although mutations in NEMO have not been associated with IBD, considering that anti-TNF therapy is highly effective in the treatment of CD and UC and reduces epithelial cell death (Zeissig et al., 2004), it is tempting to speculate that RIPK1 kinase activity might contribute to the pathogenic role of TNF in human IBD patients by triggering intestinal epithelial cell death. In the absence of evidence that RIPK1-induced epithelial cell death occurs and is functionally

Figure 6. Lack of RIPK1 Kinase Activity Prevents Colitis Development and Paneth Cell Loss in NEMO^{IEC-KO} Mice

(A and E) Representative images of colon and ileal sections from mice with the indicated genotypes.

(B and F) Graphs depicting histopathological scores of colon and ileal sections from mice with the indicated genotypes (n = 6–13 mice per genotype).

(C and I) Graphs depicting the percentage of crypts with cl. casp. 3 stained cells on colon and ileal sections from littermates with the indicated genotypes (n = 4–12 mice per genotype).

(D, H) Graphs depicting mRNA levels of the indicated genes in the colon and ileum of mice with the indicated genotypes (n = 6 or 7 mice per genotype).

(G) Graph depicting Paneth cell scores of ileal sections from mice with the indicated genotypes (n = 6–10 mice per genotype).

(J) Immunoblot analysis of the indicated proteins co-immunoprecipitated with FADD from total colon lysates from mice with the indicated genotypes (one out of three independent experiments shown).

Scale bars represent 100 μm.

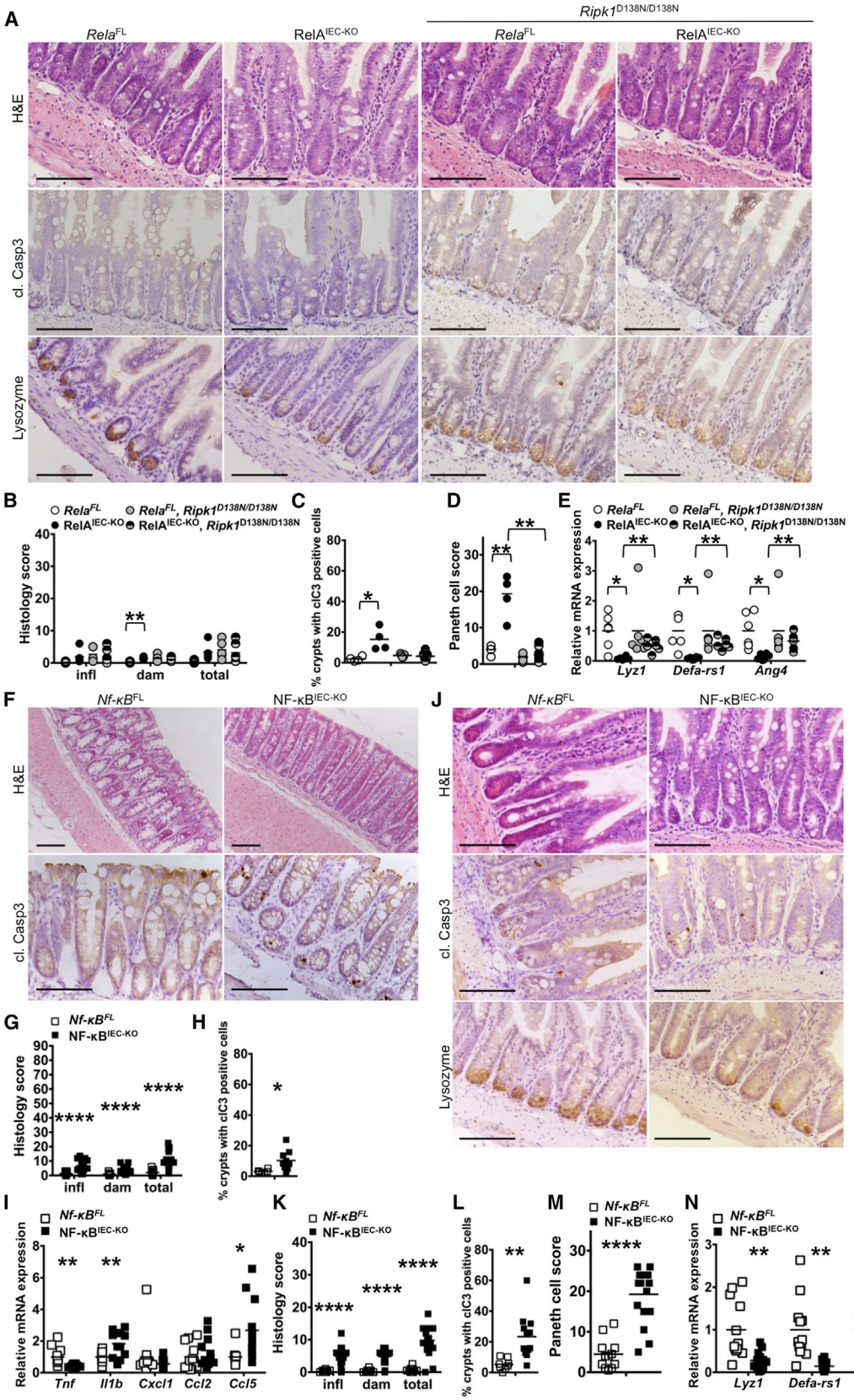

(legend on next page)

relevant for the pathogenesis of IBD, this remains an interesting hypothesis that awaits experimental validation.

EXPERIMENTAL PROCEDURES

Mice

Mice were maintained at the SPF animal facilities of the Institute for Genetics and the CECAD Research Center, University of Cologne, under a 12 hr light cycle and were given a regular chow diet (Harlan, diet no. 2918) and water ad libitum. Germ-free mice were produced at the gnotobiotic facility of the University of Ulm. All animal procedures were conducted in accordance with European, national, and institutional guidelines, and protocols were approved by local government authorities (Landesamt für Natur, Umwelt und Verbraucherschutz Nordrhein-Westfalen). Animals requiring medical attention were provided with appropriate care and excluded from the experiments described. No other exclusion criteria existed. Detailed description can be found in the Supplemental Information.

IEC Isolation and Immunoblotting

IECs were isolated by subsequent incubation of intestinal tissue in 1 mM dithiothreitol (DTT) and 1.5 mM EDTA solutions as described previously (Dannappel et al., 2014). Cell lysis buffer was supplemented with protease and phosphatase inhibitor tablets (Roche). Cell lysates were separated on SDS-PAGE and transferred to PVDF membranes (IPVH00010, Millipore). Primary antibodies used for immunoblot analysis: RelA C-20 (sc-372), RelB C-19 (sc-226), and c-Rel (sc-71), β-actin 1-19 (sc-161) and HDAC1 H-51 (sc-7872) from Santa Cruz, TNFR1 (D317K); Caspase 3 (9662), cleaved Caspase 3 (9661) from Cell Signaling; RIPK1 (610459) from BD; RIPK3 (ADI-905-242-100) from Enzo Life Sciences; FADD (1F7) 05-486 from Upstate; Cre 69050-3 from Novagen; Caspase-8 (ALX-804-447) from Alexis; and NEMO (homemade rabbit polyclonal serum) and α-tubulin (T6074) from Sigma. Secondary HRP-coupled antibodies (GE Healthcare, Jackson Immuno Research) and chemiluminescent detection substrate (GE Healthcare and Thermo Scientific) were used. For immunoprecipitation, colon tissue was lysed in IP buffer and FADD was precipitated with goat anti-FADD (M19) (sc-6036) antibody from Santa Cruz linked to protein G Dynabeads (Life Technologies). After extensive washes, beads were boiled in SDS-containing sample buffer.

Histology and Immunohistochemistry

Intestinal tissues were fixed in 4% paraformaldehyde, embedded in paraffin, and cut in 3 μm sections. For histopathological analysis, hematoxylin and eosin staining was performed according to standard protocol. For immunohistochemical (IHC) staining paraffin sections were rehydrated and heat-induced antigen retrieval was performed in citrate buffer at pH 6.0. Primary antibodies for IHC were anti-cleaved caspase 3 Asp175 (9661, Cell Signaling), anti-human lysozyme (F0372, Dako) and RelA C-20 (sc-372), Santa Cruz. Biotinylated secondary antibodies were purchased from Perkin Elmer and Dako. Stainings were visualized with ABC Kit Vectastain Elite (Vector Laboratories) or Streptavidin-HRP (Millipore) and DAB substrate (DAKO and Vector Laboratories). Incubation times with DAB substrate were equal for all samples. Histopathological evaluation of tissue sections was performed as described in the Supplemental Information.

Intestinal Organoid Culture

Small intestinal organoids were isolated and cultured as described previously (Dannappel et al., 2014). After passaging, cultures were grown for 2 to 3 days and stimulated with 5 ng/ml recombinant murine TNF. At indicated time points, cultures were collected for RNA extraction.

Statistics

Statistical analysis was performed with Prism6, GraphPad applying Student's t tests with Welch's correction in case of unequal variance. *$p \leq 0.05$; **$p \leq 0.01$; ***$p \leq 0.005$;****$p \leq 0.0001$.

SUPPLEMENTAL INFORMATION

Supplemental Information includes six figures and Supplemental Experimental Procedures and can be found with this article online at http://dx.doi.org/10.1016/j.immuni.2016.02.020.

AUTHOR CONTRIBUTIONS

K.V. and A.W. performed the experiments and analyzed data. A.P. generated the *Ripk1*$^{D138N/D138N}$ mice and performed and analyzed the *Nemo*$^{-/-}$ *Ripk1*$^{D138N/D138N}$ crosses. V.K. performed and analyzed immunoprecipitation experiments and the *RelA*$^{-/-}$ *Ripk1*$^{D138N/D138N}$ crosses. M.D. evaluated cleaved caspase-3 stainings. R.S. performed FACS analysis of IECs. P.W. generated and initially characterized NEMO$^{IEC\text{-}KO}$ FADD$^{IEC\text{-}KO}$ *Ripk3*$^{-/-}$ mice. T.C. performed qRT-PCR analysis. M.K. designed and generated the targeting constructs for *Ripk1*$^{D138N/D138N}$ mice. H.W. contributed *Traillr*^{FL} mice, F.W. contributed *RelB*^{FL} mice, and U.K. contributed *c-Rel*^{FL} mice. M.P. coordinated the project and together with K.V. wrote the paper.

ACKNOWLEDGMENTS

We are grateful to V. Dixit and Genentech for *Ripk3*$^{-/-}$, G. Kollias for *Tnfr1*^{FL}, D. Gumucio for Villin-Cre, and S. Robine for Villin-CreER^{T2} mice, and to P. Kirsch and the gnotobiotic facility at the University of Ulm for the generation of germ-free NEMO$^{IEC\text{-}KO}$ mice. We thank J. Buchholz, C. Uthoff-Hachenberg, E. Mahlberg, B. Kühnel, B. Hülser, E. Stade, and D. Beier for technical assistance. Research reported in this publication was supported by funding from the ERC (grant agreement no. 323040), the DFG (SFB670, SPP1656), and the European Commission (grants 223404 and 223151) to M.P., and by the NIAID division of the NIH under award RO1AI075118 to M.K.

Received: April 22, 2015
Revised: October 25, 2015
Accepted: December 14, 2015
Published: March 15, 2016

REFERENCES

Alcamo, E., Mizgerd, J.P., Horwitz, B.H., Bronson, R., Beg, A.A., Scott, M., Doerschuk, C.M., Hynes, R.O., and Baltimore, D. (2001). Targeted mutation of TNF receptor I rescues the RelA-deficient mouse and reveals a critical role for NF-kappa B in leukocyte recruitment. J. Immunol. *167*, 1592–1600.

Blumberg, R., and Powrie, F. (2012). Microbiota, disease, and back to health: a metastable journey. Sci. Transl. Med. *4*, 137rv7.

Dannappel, M., Vlantis, K., Kumari, S., Polykratis, A., Kim, C., Wachsmuth, L., Eftychi, C., Lin, J., Corona, T., Hermance, N., et al. (2014). RIPK1 maintains epithelial homeostasis by inhibiting apoptosis and necroptosis. Nature *513*, 90–94.

Figure 7. Epithelial NF-κB Deficiency Does Not Trigger Colitis but Causes RIPK1 Kinase Dependent Paneth Cell Death

(A, F, and J) Representative images of colon and ileal sections from mice with the indicated genotypes.
(B, G, and K) Graphs depicting histopathological scores of colon and ileal sections from mice with the indicated genotypes (n = 5–18 mice per genotype).
(C, H, and L) Graphs depicting the percentage of crypts with cl. casp. 3 stained cells on colon and ileal sections from littermates with the indicated genotypes (n = 4–12 mice per genotype).
(D and M) Graphs depicting Paneth cell scores of ileal sections from mice with the indicated genotypes (n = 4–12 mice per genotype).
(E, I, and N) Graphs depicting mRNA levels of the indicated genes in the colon and ileum of mice with the indicated genotypes (n = 5–12 mice per genotype).
Scale bars represent 100 μm. See also Figures S5 and S6.

Dillon, C.P., Weinlich, R., Rodriguez, D.A., Cripps, J.G., Quarato, G., Gurung, P., Verbist, K.C., Brewer, T.L., Llambi, F., Gong, Y.N., et al. (2014). RIPK1 blocks early postnatal lethality mediated by caspase-8 and RIPK3. Cell *157*, 1189–1202.

Dondelinger, Y., Jouan-Lanhouet, S., Divert, T., Theatre, E., Bertin, J., Gough, P.J., Giansanti, P., Heck, A.J., Dejardin, E., Vandenabeele, P., and Bertrand, M.J. (2015). NF-κB-Independent Role of IKKα/IKKβ in Preventing RIPK1 Kinase-Dependent Apoptotic and Necroptotic Cell Death during TNF Signaling. Mol. Cell *60*, 63–76.

Eckmann, L., Nebelsiek, T., Fingerle, A.A., Dann, S.M., Mages, J., Lang, R., Robine, S., Kagnoff, M.F., Schmid, R.M., Karin, M., et al. (2008). Opposing functions of IKKbeta during acute and chronic intestinal inflammation. Proc. Natl. Acad. Sci. USA *105*, 15058–15063.

Fish, J.D., Duerst, R.E., Gelfand, E.W., Orange, J.S., and Bunin, N. (2009). Challenges in the use of allogeneic hematopoietic SCT for ectodermal dysplasia with immune deficiency. Bone Marrow Transplant. *43*, 217–221.

Hanson, E.P., Monaco-Shawver, L., Solt, L.A., Madge, L.A., Banerjee, P.P., May, M.J., and Orange, J.S. (2008). Hypomorphic nuclear factor-kappaB essential modulator mutation database and reconstitution system identifies phenotypic and immunologic diversity. J Allergy Clin Immunol *122*, 1169–1177.e1116.

Hooper, L.V., Littman, D.R., and Macpherson, A.J. (2012). Interactions between the microbiota and the immune system. Science *336*, 1268–1273.

Ireland, H., Houghton, C., Howard, L., and Winton, D.J. (2005). Cellular inheritance of a Cre-activated reporter gene to determine Paneth cell longevity in the murine small intestine. Dev. Dyn. *233*, 1332–1336.

Kang, T.B., Yang, S.H., Toth, B., Kovalenko, A., and Wallach, D. (2013). Caspase-8 blocks kinase RIPK3-mediated activation of the NLRP3 inflammasome. Immunity *38*, 27–40.

Karin, M., and Greten, F.R. (2005). NF-kappaB: linking inflammation and immunity to cancer development and progression. Nat. Rev. Immunol. *5*, 749–759.

Kaser, A., Zeissig, S., and Blumberg, R.S. (2010). Inflammatory bowel disease. Annu. Rev. Immunol. *28*, 573–621.

Kawai, T., Nishikomori, R., and Heike, T. (2012). Diagnosis and treatment in anhidrotic ectodermal dysplasia with immunodeficiency. Allergol. Int. *61*, 207–217.

Lawlor, K.E., Khan, N., Mildenhall, A., Gerlic, M., Croker, B.A., D'Cruz, A.A., Hall, C., Kaur Spall, S., Anderton, H., Masters, S.L., et al. (2015). RIPK3 promotes cell death and NLRP3 inflammasome activation in the absence of MLKL. Nat. Commun. *6*, 6282.

Legarda-Addison, D., Hase, H., O'Donnell, M.A., and Ting, A.T. (2009). NEMO/IKKgamma regulates an early NF-kappaB-independent cell-death checkpoint during TNF signaling. Cell Death Differ. *16*, 1279–1288.

Mizukami, T., Obara, M., Nishikomori, R., Kawai, T., Tahara, Y., Sameshima, N., Marutsuka, K., Nakase, H., Kimura, N., Heike, T., and Nunoi, H. (2012). Successful treatment with infliximab for inflammatory colitis in a patient with X-linked anhidrotic ectodermal dysplasia with immunodeficiency. J. Clin. Immunol. *32*, 39–49.

Moriwaki, K., Balaji, S., McQuade, T., Malhotra, N., Kang, J., and Chan, F.K. (2014). The necroptosis adaptor RIPK3 promotes injury-induced cytokine expression and tissue repair. Immunity *41*, 567–578.

Nenci, A., Becker, C., Wullaert, A., Gareus, R., van Loo, G., Danese, S., Huth, M., Nikolaev, A., Neufert, C., Madison, B., et al. (2007). Epithelial NEMO links innate immunity to chronic intestinal inflammation. Nature *446*, 557–561.

O'Donnell, M.A., Hase, H., Legarda, D., and Ting, A.T. (2012). NEMO inhibits programmed necrosis in an NFκB-independent manner by restraining RIP1. PLoS ONE *7*, e41238.

Oeckinghaus, A., and Ghosh, S. (2009). The NF-kappaB family of transcription factors and its regulation. Cold Spring Harb. Perspect. Biol. *1*, a000034.

Ouellette, A.J. (2010). Paneth cells and innate mucosal immunity. Curr. Opin. Gastroenterol. *26*, 547–553.

Pai, S.Y., Levy, O., Jabara, H.H., Glickman, J.N., Stoler-Barak, L., Sachs, J., Nurko, S., Orange, J.S., and Geha, R.S. (2008). Allogeneic transplantation successfully corrects immune defects, but not susceptibility to colitis, in a patient with nuclear factor-kappaB essential modulator deficiency. J Allergy Clin Immunol *122*, 1113–1118.e1111.

Pasparakis, M. (2009). Regulation of tissue homeostasis by NF-kappaB signalling: implications for inflammatory diseases. Nat. Rev. Immunol. *9*, 778–788.

Pasparakis, M., and Vandenabeele, P. (2015). Necroptosis and its role in inflammation. Nature *517*, 311–320.

Permaul, P., Narla, A., Hornick, J.L., and Pai, S.Y. (2009). Allogeneic hematopoietic stem cell transplantation for X-linked ectodermal dysplasia and immunodeficiency: case report and review of outcomes. Immunol. Res. *44*, 89–98.

Peyrin-Biroulet, L. (2010). Anti-TNF therapy in inflammatory bowel diseases: a huge review. Minerva Gastroenterol. Dietol. *56*, 233–243.

Polykratis, A., Hermance, N., Zelic, M., Roderick, J., Kim, C., Van, T.M., Lee, T.H., Chan, F.K., Pasparakis, M., and Kelliher, M.A. (2014). Cutting edge: RIPK1 Kinase inactive mice are viable and protected from TNF-induced necroptosis in vivo. J. Immunol. *193*, 1539–1543.

Rickard, J.A., O'Donnell, J.A., Evans, J.M., Lalaoui, N., Poh, A.R., Rogers, T., Vince, J.E., Lawlor, K.E., Ninnis, R.L., Anderton, H., et al. (2014). RIPK1 regulates RIPK3-MLKL-driven systemic inflammation and emergency hematopoiesis. Cell *157*, 1175–1188.

Seidelin, J.B., and Nielsen, O.H. (2009). Epithelial apoptosis: cause or consequence of ulcerative colitis? Scand. J. Gastroenterol. *44*, 1429–1434.

Souza, H.S., Tortori, C.J., Castelo-Branco, M.T., Carvalho, A.T., Margallo, V.S., Delgado, C.F., Dines, I., and Elia, C.C. (2005). Apoptosis in the intestinal mucosa of patients with inflammatory bowel disease: evidence of altered expression of FasL and perforin cytotoxic pathways. Int. J. Colorectal Dis. *20*, 277–286.

Steinbrecher, K.A., Harmel-Laws, E., Sitcheran, R., and Baldwin, A.S. (2008). Loss of epithelial RelA results in deregulated intestinal proliferative/apoptotic homeostasis and susceptibility to inflammation. J. Immunol. *180*, 2588–2599.

Takahashi, N., Vereecke, L., Bertrand, M.J., Duprez, L., Berger, S.B., Divert, T., Gonçalves, A., Sze, M., Gilbert, B., Kourula, S., et al. (2014). RIPK1 ensures intestinal homeostasis by protecting the epithelium against apoptosis. Nature *513*, 95–99.

Van Hauwermeiren, F., Armaka, M., Karagianni, N., Kranidioti, K., Vandenbroucke, R.E., Loges, S., Van Roy, M., Staelens, J., Puimège, L., Palagani, A., et al. (2013). Safe TNF-based antitumor therapy following p55TNFR reduction in intestinal epithelium. J. Clin. Invest. *123*, 2590–2603.

Wang, X., Jiang, W., Yan, Y., Gong, T., Han, J., Tian, Z., and Zhou, R. (2014). RNA viruses promote activation of the NLRP3 inflammasome through a RIP1-RIP3-DRP1 signaling pathway. Nat. Immunol. *15*, 1126–1133.

Welz, P.S., Wullaert, A., Vlantis, K., Kondylis, V., Fernández-Majada, V., Ermolaeva, M., Kirsch, P., Sterner-Kock, A., van Loo, G., and Pasparakis, M. (2011). FADD prevents RIP3-mediated epithelial cell necrosis and chronic intestinal inflammation. Nature *477*, 330–334.

Zaph, C., Troy, A.E., Taylor, B.C., Berman-Booty, L.D., Guild, K.J., Du, Y., Yost, E.A., Gruber, A.D., May, M.J., Greten, F.R., et al. (2007). Epithelial-cell-intrinsic IKK-beta expression regulates intestinal immune homeostasis. Nature *446*, 552–556.

Zeissig, S., Bojarski, C., Buergel, N., Mankertz, J., Zeitz, M., Fromm, M., and Schulzke, J.D. (2004). Downregulation of epithelial apoptosis and barrier repair in active Crohn's disease by tumour necrosis factor alpha antibody treatment. Gut *53*, 1295–1302.

Immunity, Volume *44*

Supplemental Information

NEMO Prevents RIP Kinase 1-Mediated Epithelial Cell Death and Chronic Intestinal Inflammation by NF-κB-Dependent and -Independent Functions

Katerina Vlantis, Andy Wullaert, Apostolos Polykratis, Vangelis Kondylis, Marius Dannappel, Robin Schwarzer, Patrick Welz, Teresa Corona, Henning Walczak, Falk Weih, Ulf Klein, Michelle Kelliher, and Manolis Pasparakis

Supplemental Data Figure 1

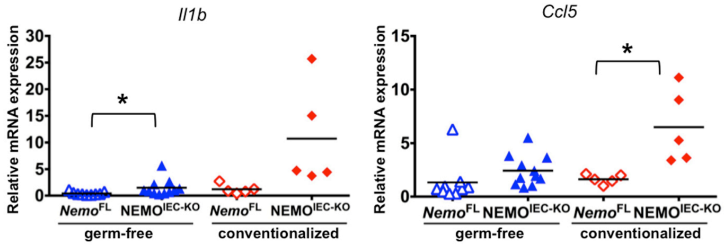

Figure S1 related to Figure 1

Inflammatory cytokine expression in NEMO^{IEC-KO} colons is driven by the microbiota

Graphs depicting relative mRNA expression levels of the indicated genes in colons of germ-free and conventionalized NEMO^{IEC-KO} and *Nemo*^{FL} mice (n = 5-11 mice per genotype).

Supplemental Data Figure 2

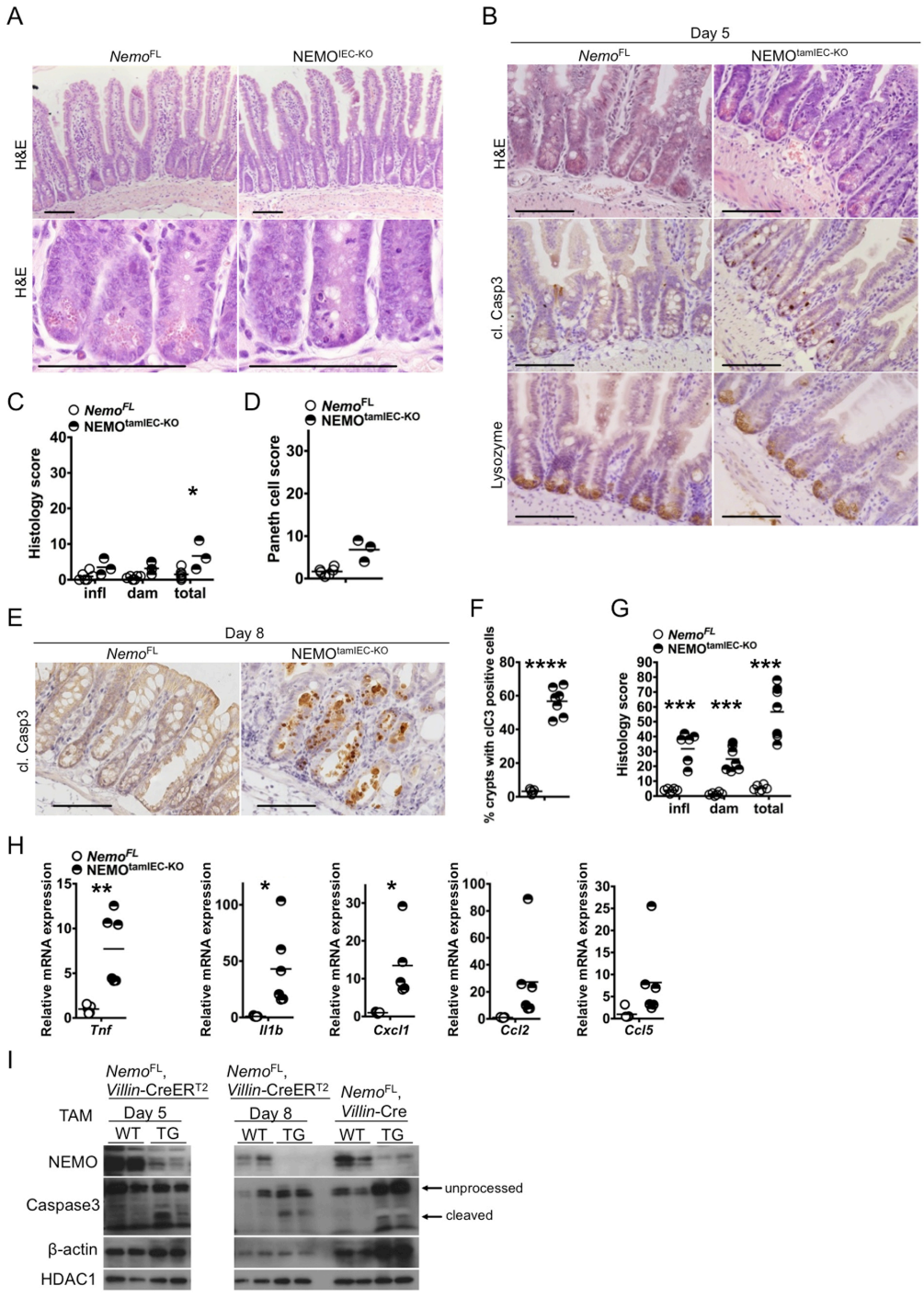

Figure S2 related to Figure 2

Paneth cell deficiency in NEMO^{IEC-KO} mice is a consequence of cell death

(A) Representative microscopy pictures of ileal sections from NEMO^{IEC-KO} and *Nemo*^{FL} mice stained with H&E at low and high power magnification.

(B) Representative images of ileal sections from NEMO$^{tamIEC-KO}$ and *Nemo*^{FL} mice 5 days after tamoxifen administration.

(C) Graph depicting histopathological scores of ileal sections from NEMO$^{tamIEC-KO}$ and *Nemo*^{FL} mice 5 days after tamoxifen administration (n = 3-6 mice per genotype).

(D) Graph depicting Paneth cell scores of ileal sections from NEMO$^{tamIEC-KO}$ and *Nemo*^{FL} mice 5 days after tamoxifen administration (n = 3-6 mice per genotype).

(E) Representative images of colon sections from NEMO$^{tamIEC\text{-}KO}$ and *Nemo*^{FL} mice on day 8 of tamoxifen administration immunostained for cl. casp3.

(F) Graph depicting percentage of crypts with cl. casp. 3 stained cells on colon sections of NEMO$^{tamIEC\text{-}KO}$ and *Nemo*^{FL} mice 8 days after tamoxifen administration (n = 5-6 mice per genotype).

(G) Graph depicting histopathological scores of colon sections from NEMO$^{tamIEC\text{-}KO}$ and *Nemo*^{FL} mice 8 days after tamoxifen administration (n = 6-7 mice per genotype).

(H) Graphs depicting mRNA levels of the indicated genes in the colon of NEMO$^{tamIEC\text{-}KO}$ and *Nemo*^{FL} littermates 8 days after tamoxifen administration (n = 5-6 mice per genotype).

(I) Immunoblot analysis of protein extracts from primary colon IECs from NEMO$^{tamIEC\text{-}KO}$ and *Nemo*^{FL} littermates 5 and 8 days after tamoxifen administration, and from *Nemo*^{FL} and NEMO $^{IEC\text{-}KO}$ mice probed with the indicated antibodies.

All scale bars represent 100μm.

Supplemental Data Figure 3

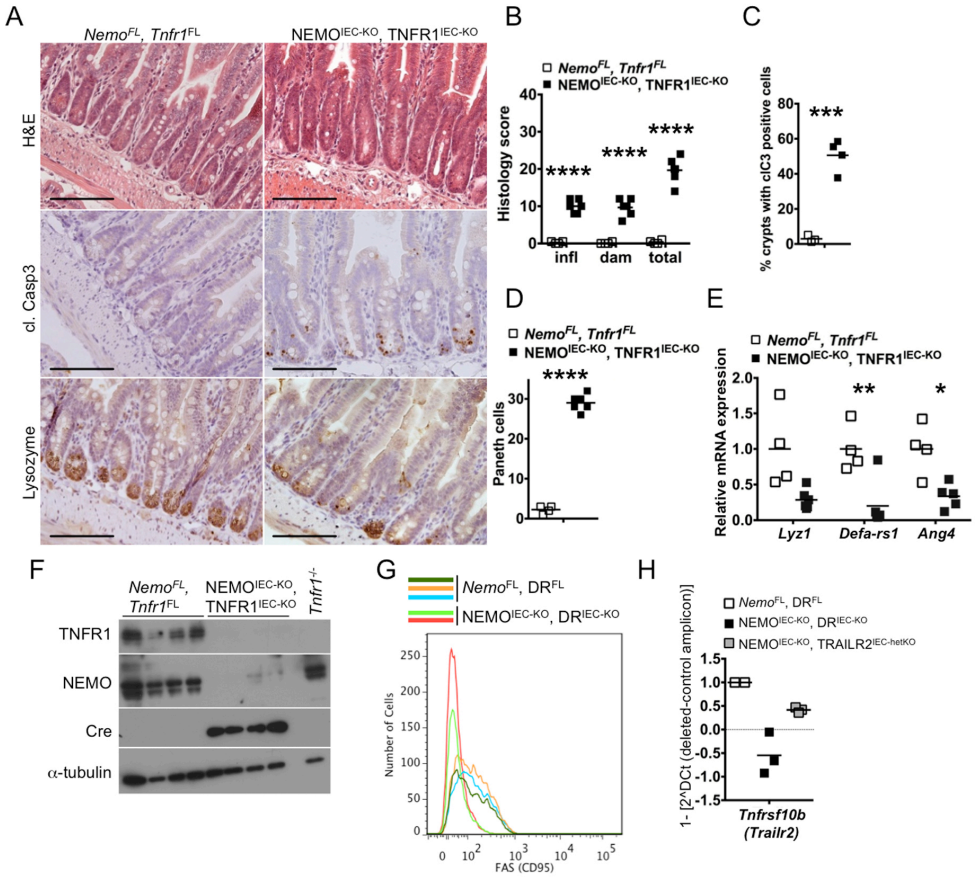

Figure S3 related to Figure 3

Deficiency of Paneth cells in NEMO^{IEC-KO} mice is not mediated by TNFR1 induced cell death

(A) Representative images of ileal sections from NEMO^{IEC-KO}, TNFR1^{IEC-KO} and *Nemo*^{FL}, *Tnfr1*^{FL} mice stained with H&E or immunostained for cl. casp3 or lysozyme.

(B) Graph depicting histopathological scores of ileal sections from NEMO^{IEC-KO}, TNFR1^{IEC-KO} and *Nemo*^{FL}, *Tnfr1*^{FL} mice (n = 4-6 mice per genotype).

(C) Graph depicting percentage of crypts with cl. casp 3 stained cells on ileal sections from NEMO^{IEC-KO}, TNFR1^{IEC-KO} and *Nemo*^{FL}, *Tnfr1*^{FL} mice (n = 3-4 mice per genotype).

(D) Graph depicting Paneth cell scores of ileal sections from NEMO^{IEC-KO}, TNFR1^{IEC-KO} and *Nemo*^{FL}, *Tnfr1*^{FL} mice (n = 4-6 mice per genotype).

(E) Graph depicting mRNA levels of the indicated genes in the ileum of NEMO^{IEC-KO}, TNFR1^{IEC-KO} and *Nemo*^{FL}, *Tnfr1*^{FL} mice (n = 4-6 mice per genotype).

(F) Immunoblot analysis of protein extracts from primary small intestinal IECs from NEMO^{IEC-KO}, TNFR1^{IEC-KO} and *Nemo*^{FL}, *Tnfr1*^{FL} mice with the indicated antibodies.

(G) Plot showing FAS (CD95) expression on primary small intestinal IECs (EpCAM^{high} living cells) from mice with the indicated genotypes as assessed by FACS (n = 2-3 mice per genotype).

(H) Relative deletion of the loxP flanked sequence in the *Tnfrsf10b* (*Trailr2)* coding region in genomic DNA from small intestinal IECs of 2 to 3 mice with the indicated genotypes, as assessed by the relative amplification of the deleted locus area versus a control genomic region.

All scale bars represent 100µm.

Supplemental Data Figure 4

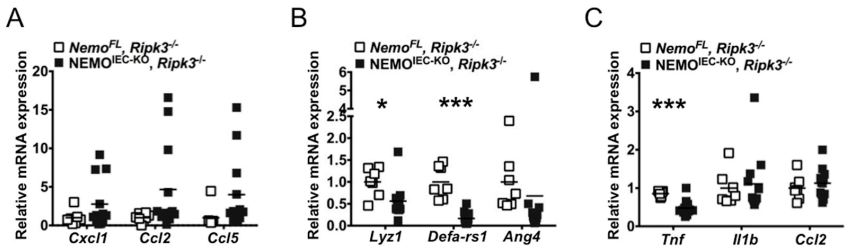

Figure S4 related to Figure 5

Deletion of RIPK3 ameliorates inflammation in colons of NEMO^{IEC-KO} mice but does not affect Paneth cell deficiency

(A) Graph depicting mRNA levels of the indicated genes in the colon of NEMO^{IEC-KO}, *Ripk3*$^{-/-}$ and *Nemo*^{FL}, *Ripk3*$^{-/-}$ mice (n = 8-12 mice per genotype).

(B, C) Graphs depicting mRNA levels of the indicated genes in the ileum of NEMO^{IEC-KO}, *Ripk3*$^{-/-}$ and *Nemo*^{FL}, *Ripk3*$^{-/-}$ mice (n = 7-12 mice per genotype).

Supplemental Data Figure 5

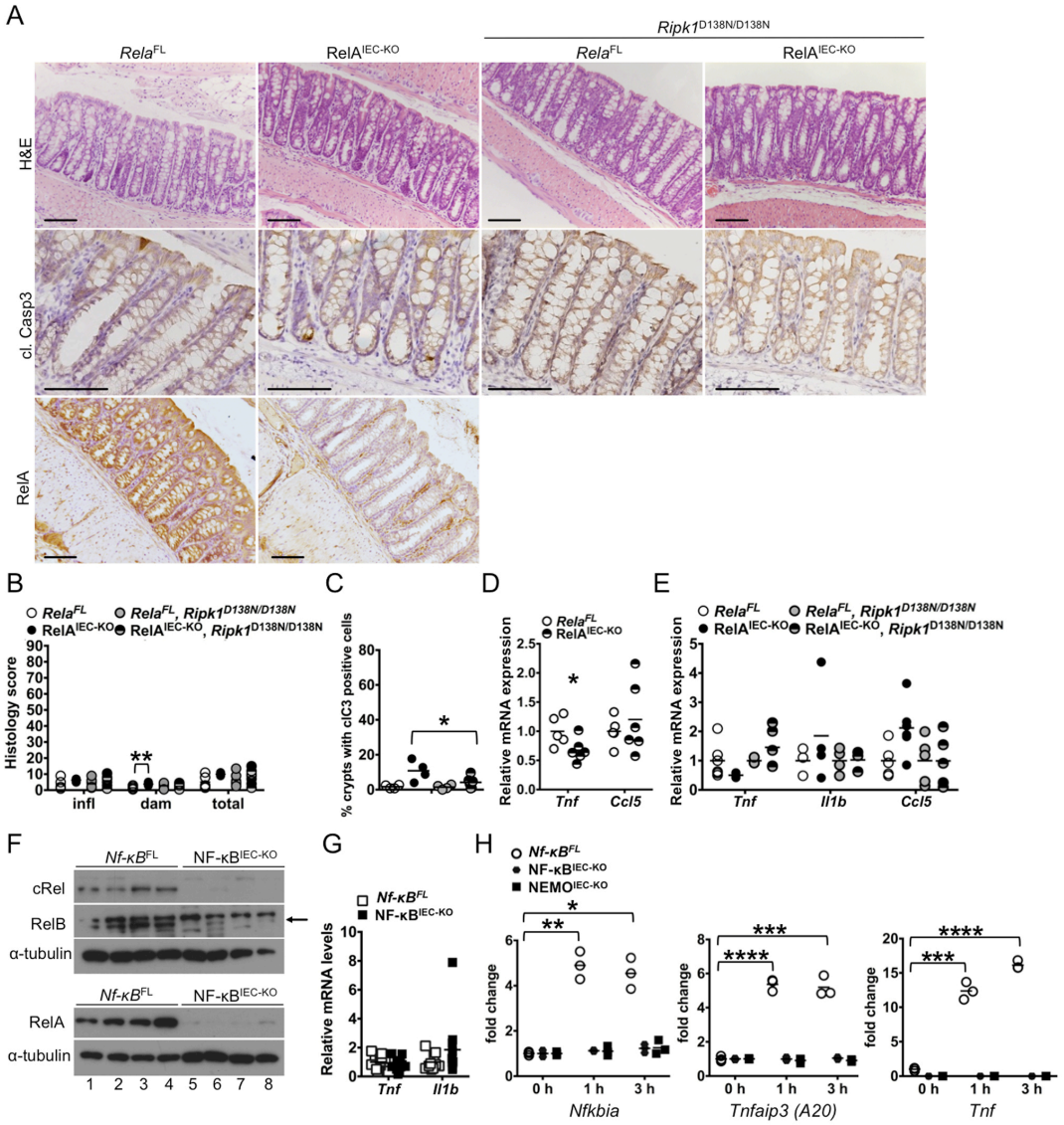

Figure S5 related to Figure 7

RelA$^{IEC\text{-}KO}$ mice do not develop spontaneous colitis

(A) Representative images of colon sections from RelA$^{IEC\text{-}KO}$ and *Rela*^{FL} littermates and RelA$^{IEC\text{-}KO}$, *Ripk1*$^{D138N/D138N}$ and *Rela*^{FL}, *Ripk1*$^{D138N/D138N}$ littermate mice stained with H&E or immunostained for cl. casp3 or RelA.

(B) Graph depicting histopathological scores of colon sections from RelA$^{IEC\text{-}KO}$ and *Rela*^{FL} littermates and RelA$^{IEC\text{-}KO}$, *Ripk1*$^{D138N/D138N}$ and *Rela*^{FL}, *Ripk1*$^{D138N/D138N}$ littermate mice (n = 5-6 mice per genotype).

(C) Graph depicting percentage of crypts with cl. casp. 3 stained cells on colon sections from RelA$^{IEC\text{-}KO}$ and *Rela*^{FL}, RelA$^{IEC\text{-}KO}$, *Ripk1*$^{D138N/D138N}$ and *Rela*^{FL}, *Ripk1*$^{D138N/D138N}$ mice (n = 4-6 mice per genotype).

(D) Graph depicting mRNA levels of the indicated genes in the colon of RelA$^{IEC\text{-}KO}$ and *Rela*^{FL} mice (n = 5-6 mice per genotype).

(E) Graph depicting mRNA levels of the indicated genes in ilea from RelA$^{IEC\text{-}KO}$, *Rela*^{FL}, RelA$^{IEC\text{-}KO}$, *Ripk1*$^{D138N/D138N}$ and *Rela*^{FL}, *Ripk1*$^{D138N/D138N}$ mice (n = 3-6 mice per genotype).

(F) Immunoblot analysis of protein extracts from primary small intestinal IECs from *Nf-κB*^{FL} and NF-κB$^{IEC\text{-}KO}$ mice with the indicated antibodies. Note that the extract in line 6 is derived from a heterozygous *relb*$^{FL/WT}$ mouse thus showing reduced levels of RelB protein. Arrow indicates specific band for RelB.

(G) Graph depicting mRNA levels of the indicated genes in the ileum of *Nf-κB*^{FL} and NF-κB$^{IEC\text{-}KO}$ littermates (n = 11-12 mice per genotype).

(H) Graphs depicting the fold change of mRNA levels of the indicated NF-κB target genes compared to unstimulated controls in small intestinal organoids from *Nf*-κ*B*^{FL}, NF-κB^{IEC-KO} and NEMO^{IEC-KO} mice after 1 h and 3 h stimulation with 5 ng/ml murine recombinant TNF. *Tnf* mRNA was not detectable at any time point in organoids from NF-κB^{IEC-KO} and NEMO^{IEC-KO} mice. Representative data from one of two independent experiments shown.

All scale bars represent 100μm.

Supplemental Data Figure 6

A

Parental genotypes	F: *Rela*$^{WT/-}$ X M: *Rela*$^{WT/-}$		
Born mice	expected	observed	
Genotype	%	n	%
Rela$^{WT/WT}$	25.0%	11	34.4%
Rela$^{WT/-}$	50.0%	21	65.6%
Rela$^{-/-}$	25.0%	0	0%
Total		32	
E12.5 – E14.5 Embryos	expected	observed	
Genotype	%	n	%
Rela$^{WT/WT}$	25.0%	9	28.1%
Rela$^{WT/-}$	50.0%	14	43.8%
Rela$^{-/-}$	25.0%	9	28.1%
Total		32	

B

Parental genotypes	F: *Rela*$^{WT/-}$, *Tnfr1*$^{-/-}$ X M: *Rela*$^{WT/-}$, *Tnfr1*$^{-/-}$			Day of death
Born mice	expected	observed		
Genotype	%	n	%	
Rela$^{WT/WT}$, *Tnfr1*$^{-/-}$	25.0%	4	14.3%	
Rela$^{WT/-}$, *Tnfr1*$^{-/-}$	50.0%	20	71,4%	
Rela$^{-/-}$, *Tnfr1*$^{-/-}$	25.0%	4	14.3%	P33, 3x sacrifice P2
Total		28		

C

Parental genotypes	F: *Rela*$^{WT/-}$, *Ripk1*$^{D138N/D138N}$ X M: *Rela*$^{WT/-}$, *Ripk1*$^{D138N/D138N}$			Day of death
Born mice	expected	observed		
Genotype	%	n	%	
Rela$^{WT/WT}$, *Ripk1*$^{D138N/D138N}$	25.0%	12	26.7%	
Rela$^{WT/-}$, *Ripk1*$^{D138N/D138N}$	50.0%	26	57.8%	
Rela$^{-/-}$, *Ripk1*$^{D138N/D138N}$	25.0%	7	15.6%	3x P6; P12; P27; P33; P34
Total		45		
E12.5 – E14.5 Embryos	expected	observed		
Genotype	%	n	%	
Rela$^{WT/WT}$, *Ripk1*$^{D138N/D138N}$	25.0%	12	25.5%	
Rela$^{WT/-}$, *Ripk1*$^{D138N/D138N}$	50.0%	25	53.2%	
Rela$^{-/-}$, *Ripk1*$^{D138N/D138N}$	25.0%	10	21.3%	
Total		47		

D

Parental genotypes	F: *Rela*$^{WT/-}$, *Ripk1*$^{D138N/WT}$ X M: *Rela*$^{WT/-}$, *Ripk1*$^{D138N/D138N}$			Day of death
Born mice	expected	observed		
Genotype	%	n	%	
Rela$^{WT/WT}$, *Ripk1*$^{D138N/WT}$	12.5%	8	17.0%	
Rela$^{WT/WT}$, *Ripk1*$^{D138N/D138N}$	12.5%	9	19.1%	
Rela$^{WT/-}$, *Ripk1*$^{D138N/WT}$	25.0%	13	27.7%	
Rela$^{WT/-}$, *Ripk1*$^{D138N/D138N}$	25.0%	11	23.4%	
Rela$^{-/-}$, *Ripk1*$^{D138N/WT}$	12.5%	1	2.1%	P12
Rela$^{-/-}$, *Ripk1*$^{D138N/D138N}$	12.5%	5	10.6%	P17; P15; 3x sacrifice P20
Total		43		

E

Parental genotypes	F: *Nemo*$^{WT/-}$, *Ripk1*$^{D138N/D138N}$ or F: *Nemo*$^{FL/-}$, *Ripk1*$^{D138N/D138N}$ X M: *Ripk1*$^{D138N/D138N}$		
Born male mice	expected	observed	
Genotype	%	n	%
Nemo$^{WT/Y}$, *Ripk1*$^{D138N/D138N}$ or *Nemo*$^{FL/Y}$, *Ripk1*$^{D138N/D138N}$	50.0%	8	66.7%
Nemo$^{-/Y}$, *Ripk1*$^{D138N/D138N}$	50.0%	4	33.3%
Total		12	

Figure S6 related to Figure 6 and Figure 7

RIPK1 kinase activity mediates embryonic lethality of *Rela*$^{-/-}$ and *Nemo*$^{-/-}$ mice.

(A) Table showing the expected Mendelian frequency and the observed frequency of born offspring and E12.5-E14.5 embryos with the indicated genotypes from matings with *Rela*$^{WT/-}$ female (F) and *Rela*$^{WT/-}$ male (M) mice.

(B) Table showing the expected Mendelian frequency and the observed frequency of born offspring with the indicated genotypes from matings with *Rela*$^{WT/-}$, *Tnfr1*$^{-/-}$ female (F) and *Rela*$^{WT/-}$, *Tnfr1*$^{-/-}$ male (M) mice. The last column indicates the day of death or day of sacrifice of *Rela*$^{-/-}$, *Tnfr1*$^{-/-}$ offspring.

(C) Table showing the expected Mendelian frequency and the observed frequency of born offspring and E12.5-E14.5 embryos with the indicated genotypes from matings with *Rela*$^{WT/-}$, *Ripk1*$^{D138N/D138N}$ female (F) and *Rela*$^{WT/-}$, *Ripk1*$^{D138N/D138N}$ male (M) mice. The last column indicates the day of death or day of sacrifice of *Rela*$^{-/-}$, *Ripk1*$^{D138N/D138N}$ mice.

(D) Table showing the expected Mendelian frequency and the observed frequency of born offspring with the indicated genotypes from matings with *Rela*$^{WT/-}$, *Ripk1*$^{WT/D138N}$ female (F) and *Rela*$^{WT/-}$, *Ripk1*$^{D138N/D138N}$ male (M) mice. The last column indicates the day of death or day of sacrifice of *Rela*$^{-/-}$, *Ripk1*$^{D138N/D138N}$ and *Rela*$^{-/-}$, *Ripk1*$^{WT/D138N}$ mice.

(E) Table showing the expected Mendelian frequency and the observed frequency of born male offspring with the indicated genotypes from *Nemo*$^{WT/-}$, *Ripk1*$^{D138N/D138N}$ or *Nemo*$^{FL/-}$, *Ripk1*$^{D138N/D138N}$ females (F) mated to *Ripk1*$^{D138N/138N}$ males (M). *Nemo*$^{-/Y}$; *Ripk1*$^{D138N/D138N}$ pups were dead by P3.

Supplemental Experimental Procedures

Mice

Nemo^{FL} (*Ikbkg*^{fl}) (Schmidt-Supprian et al., 2000), *Rela*^{FL} (Luedde et al., 2008), *Fadd*^{FL} (Welz et al., 2011) and *Ripk1*$^{D138N/D138N}$ mice (Polykratis et al., 2014) were generated by gene targeting in C57BL/6 ES cells. *Villin*-cre (Madison et al., 2002), *Villin*-creER^{T2} (el Marjou et al., 2004), *Tnfr1*^{FL} (*Tnfrsf1a*^{fl}) (Van Hauwermeiren et al., 2013), *Trailr2*^{FL} (*Tnfrsf10b*^{fl})(Grosse-Wilde et al., 2008), *Fas*^{FL} (Hao et al., 2004), *Relb*^{FL} (Powolny-Budnicka et al., 2011), *c-Rel*^{FL} (Heise et al., 2014) and *Ripk3*$^{-/-}$ mice (Newton et al., 2004) were backcrossed for at least 10 generations into the C57BL/6 genetic background. *Villin*-creER^{T2} recombinase activity was induced by 5 daily intraperitoneal administrations of 1 mg tamoxifen dissolved in corn oil/DMSO. Littermates not carrying the Cre transgenes were used as controls in all experiments. Mice were analyzed at the age of 2-4 months. Mice of the indicated genotype were assigned at random to groups. Mouse studies were performed in a blinded fashion.

Quantitative RT–PCR

Total RNA was extracted with Trizol Reagent (Life Technologies) and RNeasy Columns (Qiagen). cDNA was prepared with Superscript III cDNA-synthesis Kit (Life Technologies). qRT–PCR was performed with TaqMan probes (Life Technologies) with TATA-box-binding protein (*Tbp*) and *Gapdh* serving as reference genes. Data were analyzed according to the ΔΔCT method and are presented in dot plot graphs as fold change (relative mRNA expression) relative to Cre negative littermates. Primer sequences are available upon request.

FACS analysis of Fas expression on IECs

Small intestinal IECs were isolated as described. For viability assessment cells were stained with fixable viability dye eFluor 780 (eBioscience), epithelial cells were identified as Epcam1-high with anti-EpCAM1/CD326-FITC (eBiosience) and expression of Fas was determined with anti-Fas/CD95-PE (BD Pharmingen) antibodies. Data were acquired with LSRFortessa, BD and analysis was performed with BD FACSDiva Software v8.0, plots were prepared with FlowJo Version 7.6.5 software.

Assessment of deletion efficiency of *Trailr2*

Deletion efficiency of *Trailr2* was assessed on genomic DNA isolated from small intestinal IECs as described before (Ehlken et al., 2014). Results are depicted as 1 – [2^ - (Ct deleted amplicon – Ct control amplicon)].

Histopathological evaluation of H&E stained tissue sections

Histopathological evaluation of tissue sections was performed on 3µm H&E stained intestinal tissue sections in a blinded fashion as described previously (Adolph et al., 2013). Inflammation scores are composed of four parameters, tissue damage scores are represented by the sum of three parameters that were multiplied with a factor taking into account the fraction of tissue being affected. In brief, inflammation was assessed by the presence of infiltrating mononuclear cells, polymorphonuclear cells and lymphocytic cells (scores from 0 to 3, with 0 absent, 1 mild, 2 moderate, 3 severe), and the localization of inflammatory infiltrates (0 absent, 1 mucosal, 2 submucosal, 3 transmural extending into muscularis and serosa, and 4 diffuse). For the evaluation of tissue damage four scores were ascribed to crypt hyperplasia, epithelial injury and death of epithelial cells (0 absent, 1 mild, 2 moderate and 3 severe). The sum of these inflammation or tissue damage scores were then multiplied by a factor according to the fraction of the tissue being affected: 1, < 10%; 2, 10-25%; 3, 25-50%; and 4, >50%. The total histological score represents the sum of inflammation and damage marks.

Paneth cell scores describe morphology and abundance of Paneth cells assessed on H&E stained paraffin sections. According to the extent of morphological alterations 5 scores were used to characterize Paneth cells describing cell shape and size, and the appearance of eosinophilic secretory granules. 0 characterizes normal, differentiated Paneth cells with well-formed roundish secretory granules; a score of 1 describes mild defects in secretory granule formation and mild alterations in cell shape; 2 indicates mild alterations in cell size and shape and moderate changes in granule appearance affecting less than half of the Paneth cells within a crypt; score 3 represents Paneth cells with more overt defects in their morphology involving more than half of the Paneth cells in a crypt; score 4 characterized severe Paneth cell abnormalities clearly detectable at lower power magnifications.

Five scores were employed to characterize relative Paneth cell numbers. 0 corresponds to normal Paneth cells numbers. A score of 1 characterizes a mild reduction in Paneth cell numbers per crypt. Score 2 corresponds to up to 25% reduction of Paneth cells per crypt, already noticeable at lower power magnifications. Score 3 describes an about 50% reduction in Paneth cells with most crypts still harboring Paneth cells. 4 was assigned when remaining Paneth cells accounted for less than 30% of Paneth cells in a wild type status (score 0) and stretches of crypts devoid of Paneth cells were identified.

Supplemental References

Adolph, T.E., Tomczak, M.F., Niederreiter, L., Ko, H.J., Bock, J., Martinez-Naves, E., Glickman, J.N., Tschurtschenthaler, M., Hartwig, J., Hosomi, S.*, et al.* (2013). Paneth cells as a site of origin for intestinal inflammation. Nature *503*, 272-276.

Ehlken, H., Krishna-Subramanian, S., Ochoa-Callejero, L., Kondylis, V., Nadi, N.E., Straub, B.K., Schirmacher, P., Walczak, H., Kollias, G., and Pasparakis, M. (2014). Death receptor-independent FADD signalling triggers hepatitis and hepatocellular carcinoma in mice with liver parenchymal cell-specific NEMO knockout. Cell Death Differ *21*, 1721-1732.

el Marjou, F., Janssen, K.P., Chang, B.H., Li, M., Hindie, V., Chan, L., Louvard, D., Chambon, P., Metzger, D., and Robine, S. (2004). Tissue-specific and inducible Cre-mediated recombination in the gut epithelium. Genesis *39*, 186-193.

Grosse-Wilde, A., Voloshanenko, O., Bailey, S.L., Longton, G.M., Schaefer, U., Csernok, A.I., Schutz, G., Greiner, E.F., Kemp, C.J., and Walczak, H. (2008). TRAIL-R deficiency in mice enhances lymph node metastasis without affecting primary tumor development. J Clin Invest *118*, 100-110.

Hao, Z., Hampel, B., Yagita, H., and Rajewsky, K. (2004). T cell-specific ablation of Fas leads to Fas ligand-mediated lymphocyte depletion and inflammatory pulmonary fibrosis. J Exp Med *199*, 1355-1365.

Heise, N., De Silva, N.S., Silva, K., Carette, A., Simonetti, G., Pasparakis, M., and Klein, U. (2014). Germinal center B cell maintenance and differentiation are controlled by distinct NF-kappaB transcription factor subunits. J Exp Med *211*, 2103-2118.

Luedde, T., Heinrichsdorff, J., de Lorenzi, R., De Vos, R., Roskams, T., and Pasparakis, M. (2008). IKK1 and IKK2 cooperate to maintain bile duct integrity in the liver. Proc Natl Acad Sci U S A *105*, 9733-9738.

Madison, B.B., Dunbar, L., Qiao, X.T., Braunstein, K., Braunstein, E., and Gumucio, D.L. (2002). Cis elements of the villin gene control expression in restricted domains of the vertical (crypt) and horizontal (duodenum, cecum) axes of the intestine. J Biol Chem *277*, 33275-33283.

Newton, K., Sun, X., and Dixit, V.M. (2004). Kinase RIP3 is dispensable for normal NF-kappa Bs, signaling by the B-cell and T-cell receptors, tumor necrosis factor receptor 1, and Toll-like receptors 2 and 4. Mol Cell Biol *24*, 1464-1469.

Polykratis, A., Hermance, N., Zelic, M., Roderick, J., Kim, C., Van, T.M., Lee, T.H., Chan, F.K., Pasparakis, M., and Kelliher, M.A. (2014). Cutting edge: RIPK1 Kinase inactive mice are viable and protected from TNF-induced necroptosis in vivo. J Immunol *193*, 1539-1543.

Powolny-Budnicka, I., Riemann, M., Tanzer, S., Schmid, R.M., Hehlgans, T., and Weih, F. (2011). RelA and RelB transcription factors in distinct thymocyte populations control lymphotoxin-dependent interleukin-17 production in gammadelta T cells. Immunity *34*, 364-374.

Schmidt-Supprian, M., Bloch, W., Courtois, G., Addicks, K., Israel, A., Rajewsky, K., and Pasparakis, M. (2000). NEMO/IKK gamma-deficient mice model incontinentia pigmenti. Mol Cell *5*, 981-992.

Van Hauwermeiren, F., Armaka, M., Karagianni, N., Kranidioti, K., Vandenbroucke, R.E., Loges, S., Van Roy, M., Staelens, J., Puimege, L., Palagani, A.*, et al.* (2013). Safe TNF-based antitumor therapy following p55TNFR reduction in intestinal epithelium. J Clin Invest *123*, 2590-2603.

Welz, P.S., Wullaert, A., Vlantis, K., Kondylis, V., Fernandez-Majada, V., Ermolaeva, M., Kirsch, P., Sterner-Kock, A., van Loo, G., and Pasparakis, M. (2011). FADD prevents RIP3-mediated epithelial cell necrosis and chronic intestinal inflammation. Nature *477*, 330-334.